Hyperpolarized 3He-diffusion MRI in evaluation of lung structure in emphysema. Validation and development of the method

Diaz, Sandra

2008

Hyperpolarized ^{3}He-diffusion MRI in Evaluation of Lung Structure in Emphysema

Validation and Development of the Method

Sandra Díaz Ruiz

AKADEMISK AVHANDLING
som med vederbörligt tillstånd av Medicinska fakulteten vid Lunds universitet för avläggande av doktorsexamen i medicinsk vetenskap kommer att offentligen försvaras i CRCs aula, Universitetssjukhuset MAS, Malmö,
torsdagen den 18 december 2008, kl 09.15

Fakultetsopponent:
Professor Elna-Marie Larsson
Århus universitet, Danmark

Organization	Document name
LUND UNIVERSITY Clinical Sciences, Malmö Medical Radiology	DOCTORAL DISSERTATION
	Date of issue December 18, 2008
	Sponsoring organization
Author(s) Sandra Díaz Ruiz	

Title and subtitle

Hyperpolarized ^{3}He-diffusion MRI in Evaluation of Lung Structure in Emphysema Validation and Development of the Method

Abstract

COPD is a major cause of chronic morbidity and mortality throughout the world. It is a preventable and treatable disease. Smoking is the most commonly encountered risk factor for COPD and the habit now unfortunately starts at earlier ages than before. There is a strong necessity to diagnose COPD in early stages before symptoms present themselves. MRI with hyperpolarized ^{3}He using diffusion weighted sequences has the potential to detect and quantify parenchyma destruction in emphysema, the main manifestation of COPD.

Study I investigated the short-term reproducibility of the method and the volume of gas required to obtain suitable results in normal volunteers and patients with COPD. The mean ADC measurement was highly reproducible, sensitive to small differences in alveolar size and clearly separated volunteers and patients. There was a dependency of inhaled volume.

Study II investigated the long-term reproducibility, age-dependency and anatomical variation of ADC in normal volunteers. The mean ADC measurement was highly reproducible over one year. There was correlation between age and mean ADC. There was a difference in mean ADC between anterior and posterior parts of the lungs in supine position probably depending on the gravity.

Study III compared hyperpolarized ^{3}He-diffusion MRI technique with MSCT and different PFT:s. The mean ADC correlated well with emphysema index and 15th percentile from CT. $D_{L,CO}$ is the PFT best correlating with emphysema grade and the correlation was higher between ^{3}He -MRI and $D_{L,CO}$ than between CT and $D_{L,CO}$.

Study IV investigated if hyperpolarized ^{3}He-diffusion MRI technique was sensitive enough to detect emphysema progress over a year. The mean ADC did not detect changes over 12 months. An ad hoc analysis performed afterwards using a textural analysis, lacunarity analysis, showed progress in patients with COPD who smoked at the beginning of the study, but not in patients who had stopped smoking earlier.

In conclusion, hyperpolarized ^{3}He-diffusion MRI technique is a robust method, highly reproducible over a short and a longer period of time. The method has been validated with standard methods, pulmonary function tests and CT. The combination of MRI, hyperpolarized gases, and a proper textural analysis of the data will likely provide a powerful investigative tool at least in research settings for understanding the pathophysiology of emphysema and evaluation of therapies designed to alter the course of disease even if economic obstacles may prohibit a more widespread clinical use.

Key words:
Hyperpolarized, Helium, MRI, Emphysema, ADC

Classification system and/or index terms (if any):

Supplementary bibliographic information:	Language: English	
ISSN and key title: 1652-8220	ISBN 978-91-86059-80-4	
Recipient´s notes	Number of pages 106	Price
	Security classification	

Distribution by (name and address) **Sandra Diaz, Diagnostic Centre, University Hospital, Malmö, Sweden**

Signature  Date Oct 30, 2008

Hyperpolarized ^{3}He-diffusion MRI in Evaluation of Lung Structure in Emphysema

Validation and Development of the Method

Sandra Díaz Ruiz

LUND UNIVERSITY

To Juan and Gabriel

”I know that two and two make four -- and should be glad to prove it too if I could -- though I must say if by any sort of process I could convert 2 and 2 into five it would give me much greater pleasure.”

Lord Byron

CONTENTS

LIST OF PAPERS

The thesis is based on the following four papers, referred to in the text by their roman numerals:

I. **Hyperpolarized ^{3}He Apparent Diffusion Coefficient MRI of the lung: Reproducibility and Volume Dependency in Healthy Volunteers and Patients with Emphysema**
Sandra Diaz, Ingrid Casselbrant, Eeva Piitulainen, Göran Pettersson, Peter Magnusson, Barry Peterson, Per Wollmer, Peter Leander, Olle Ekberg and Per Åkeson
Journal of Magnetic Resonance Imaging 27:763-770 (2008)

II. **MR Imaging of Hyperpolarized Helium in Healthy Subjects: Long-term Reproducibility, Age-dependency and Anatomical Variations**
Sandra Diaz, Ingrid Casselbrant, Eeva Piitulainen, Peter Magnusson, Barry Peterson, Per Wollmer, Olle Ekberg and Per Åkeson
Submitted European Radiology

III. **Validity of Apparent Diffusion Coefficient Hyperpolarized ^{3}He-MRI Using MSCT and Pulmonary Function Tests as References**
Sandra Diaz, Ingrid Casselbrant, Eeva Piitulainen, Peter Magnusson, Barry Peterson, Per Wollmer, Peter Leander, Olle Ekberg and Per Åkeson
In Press European Journal of Radiology (2008)

IV. **Progression of Emphysema in a 12-Month Hyperpolarized ^{3}He-MRI Study: Lacunarity Analysis Provided a More Sensitive Measure than Standard ADC Analysis**
Sandra Diaz, Ingrid Casselbrant, Eeva Piitulainen, Peter Magnusson, Barry Peterson, Theresa Tuthill, Evelyn Pickering, Per Wollmer, Olle Ekberg and Per Åkeson
Submitted Academic Radiology

ABBREVIATIONS

ADC	Apparent Diffusion Coefficient
CLE	Centrilobular Emphysema
COPD	Chronic Obstructive Pulmonary Disease
CT	Computed Tomography
$D_{L,CO}$	Diffusion Capacity of Carbon Monoxide
DWI	Diffusion Weighted Imaging
$FEF_{25-75\%}$	Maximal midexpiratory flow rate
FEV_1	Forced Expiratory Volume in 1 sec
FRC	Functional Residual Capacity
FVC	Forced Vital Capacity
GRE	Gradient-echo
He	Helium
HU	Hounsfield Units
ME	Metastability Exchange
MHz	Megahertz
MRI	Magnetic Resonance Imaging
N_2	Nitrogen
NMR	Nuclear Magnetic Resonance
OPSE	Optical Pumping Spin Exchange
PFT	Pulmonary Function Test
PLE	Panlobular Emphysema
RF	Radiofrequency
RV	Residual Volume
SE	Spin-echo
TE	Echo Time
TLC	Total Lung Capacity
TR	Repetition Time
VC	Vital Capacity
^{129}Xe	Xenon

INTRODUCTION

Background

Chronic Obstructive Pulmonary Disease (COPD) is a major cause of chronic morbidity and mortality throughout the world. Many people suffer from this disease for years and die prematurely from it or its complications (1). COPD is the fourth leading cause of death in the world (2), and further increases in its prevalence and mortality can be predicted in the coming decades (3). The Global Burden of Disease Study (3, 4) has projected that COPD, which ranked sixth as the cause of death in 1990, will become the third leading cause of death worldwide by 2020.

Chronic obstructive pulmonary disease (COPD) is a preventable and treatable disease with some significant extrapulmonary effects that may contribute to the severity in individual patients. Its pulmonary component is characterized by airflow limitation that is not fully reversible. The airflow limitation is usually progressive and associated with an abnormal inflammatory response of the lung to noxious particles or gases. Worldwide, cigarette smoking is the most commonly encountered risk factor for COPD, although in many countries, air pollution resulting from the burning of wood and other biomass fuels has also been identified as a COPD risk factor. The prevalence and burden of COPD are projected to increase in the coming decades due to continued exposure to COPD risk factors and the changing age structure of the world's population (5). Inhaled cigarette smoke and other noxious particles cause lung inflammation, a normal response which appears to be amplified in patients who develop COPD. This abnormal inflammatory response may induce parenchyma destruction (resulting in emphysema), and disrupt normal repair and defence mechanisms (resulting in small airway fibrosis). These pathological changes lead to air trapping and progressive airflow limitation (1).

Emphysema

Since almost two centuries ago in 1819, when Laënec first described the structural changes of emphysema, the understanding of its different forms has evolved slowly, with many different opinions and controversies. It was not until 1959 that the world community agreed on a common morphological definition of emphysema (6).

Emphysema is defined as "a group of pulmonary diseases characterized by abnormal permanent enlargement of air spaces distal to terminal bronchioles with destruction of alveolar walls" (7-9). This definition describes emphysema as a pathological entity that is defined in strictly morphologic terms. No universally accepted classification scheme of the forms of emphysema exists. However, a histopathological

classification of the different morphological subtypes of emphysema based on the location in the secondary pulmonary lobule is the most accepted. The secondary pulmonary lobule is an important anatomic and physiologic unit of the lung supplied by three to five terminal bronchioles and separated from other lobules by fibrous septa (10-12). This structure has an irregular polyhedron form measuring 2-3 cm in diameter and contains a variable number of primary lobules (respiratory units), defined as the air space and airway distal to a respiratory bronchiole. Thus, the two major types of emphysema are *centrilobular emphysema* (CLE) and *panlobular emphysema* (PLE).

The CLE begins near the centre of the secondary pulmonary lobule in the region of the proximal respiratory bronchiole (8, 13-15). CLE is by far the most common form of emphysema and is directly related to cigarette smoking. CLE is found in up to one-half of adult smokers at autopsy (8) and has predominance in the upper and middle regions of the lungs. Various theories have tried to explain this localization. Among these, the one introduced by Pratt and Fraser (8, 13) in which the combination of diminished delivery of antiproteases, and increased negative pleural pressure in the upper lungs may explain this localization. Another theory was postulated by Cockroft et al. (16) based on the greater ventilation-perfusion ratio in the lung apices. In an upright position inhaled irritants such as cigarette smoke would be distributed in the lung in a manner similar to pulmonary ventilation, which in this position is distributed more in the upper and middle regions of the lungs.

The PLE is characterized by uniform, nonselective destruction of all air spaces throughout both lungs. Each secondary pulmonary lobule is uniformly affected from its centre to its periphery (8, 13). PLE is associated, among other things, with deficiency of serum protease inhibitor, $alpha_1$-antitrypsin and is slightly more predominant in the lower lobes. This distribution is thought to be due to the greater blood flow in the lower regions of the lungs (8, 17, 18).

Lung function

Ventilation is the process whereby the lungs replenish the gas in the alveoli. Measurements of function consist of quantification of the gas volume contained in the lungs under certain circumstances and the rate at which gas can be expelled from the lungs. Two measurements of lung volume commonly used for respiratory diagnosis are *total lung capacity* (TLC) which is the volume of gas contained in the lungs after a maximal inspiration, and *residual volume* (RV) which is the volume of gas remaining in the lungs at the end of a maximal expiration. The volume of gas that is exhaled from the lungs in going from TLC to RV is called the *vital capacity* (VC). VC is often recorded during a forced

expiration from TLC to RV (the forced vital capacity FVC). From a volume-time recording – spirogram – three measurements of airflow can be obtained: (1) the volume of gas exhaled during the first second of expiration (forced expiratory volume in 1 s, or FEV_1), (2) the FVC, and (3) the average expiratory flow rate during the middle 50 percent of the vital capacity (forced expiratory flow between 25 and 75 percent of the vital capacity, or $FEF_{25-75\%}$, also called the maximal midexpiratory flow rate). A major application of FEV_1 is the assessment of bronchial obstruction. Reductions in FEV_1 may also reflect reduction in TLC (restrictive disease of the lungs). Whereas obstruction is associated with slower emptying, reduction in TLC is associated with normal or even accelerated lung emptying. This distinction is simply assessed by measuring the ratio of FEV_1 to the FVC or to a separately obtained slow VC. Normally the FEV_1/FVC ratio is greater than 70-75% although it does fall slowly with increasing age. FEV_1 and FVC can be measured with simple devices recording expiratory flow rate. Measurements of TLC and RV require the volume of gas resident in the lungs to be measured. This is done by helium dilution or body plethysmography. The helium dilution method may underestimate the volume of gas in the lungs if there are slowly communicating airspaces, such as bullae. In this situation, lung volumes can be more accurately measured with a body plethysmograph (Fig 1).

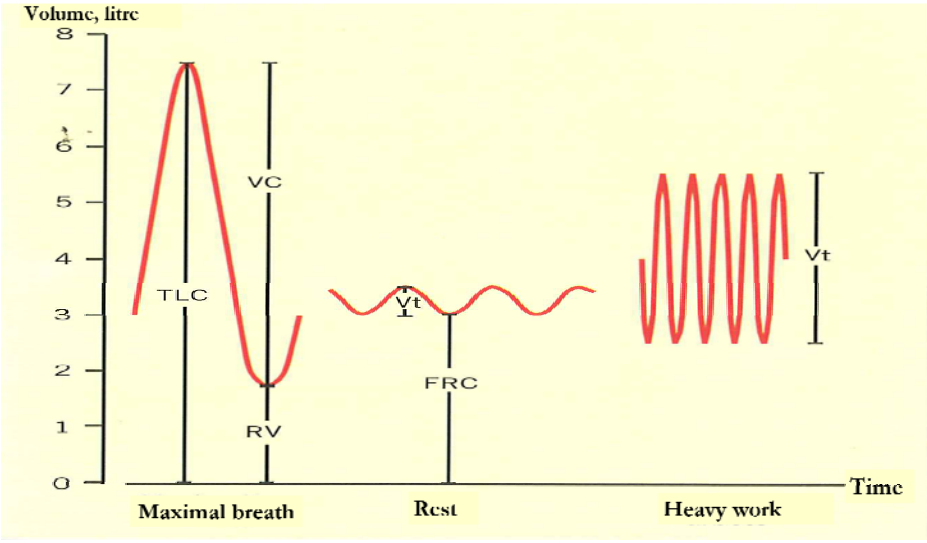

Fig 1. Lung volumes. TLC: total lung capacity. VC: Vital capacity. RV: Residual volume. FRC: Functional residual capacity. Vt: Tidal volume

The two major patterns of abnormal ventilatory function, obstructive and restrictive can be characterised using static lung volumes and spirometry. In the *obstructive pattern,* the hallmark is a decrease in expiratory flow rates. With fully establish disease, the ratio FEV_1/FVC is usually decreased. In obstructive disease, the TLC is normal or increased; RV is elevated owing to trapping of air during expiration. VC is frequently decreased because of the striking elevations in RV with only minor changes in TLC. In the *restrictive pattern* the hallmark is a decrease in lung volumes, primarily TLC and VC. RV is also generally decreased and forced expiratory flow rates are preserved with a normal FEV_1/FVC ratio.

Another important feature in lung function is the physiology of gas exchange. The primary functions of the respiratory system are to remove the appropriate amount of CO_2 from blood entering the pulmonary circulation and to provide adequate O_2 to blood leaving the pulmonary circulation. The diffusing capacity of carbon monoxide ($D_{L,CO}$) is frequently used to assess the functional integrity of the alveolar-capillary membrane, which includes the pulmonary capillary bed. $D_{L,CO}$ is usually measured with the single breath technique. The subject takes a full breath from RV to TLC of a gas mixture containing helium (He) and carbon monoxide (CO). The breath is held for 10 seconds at TLC and a sample of expired alveolar gas is analyzed for He and CO. Helium is used to correct for dilution of the inspired gas in the RV and the uptake of CO is calculated. Diseases that affect the alveolar walls of the pulmonary capillary bed will have an effect on $D_{L,CO}$. With emphysema alveolar walls are destroyed, and the surface area of the alveolar-capillary bed is thereby diminished. In *Chronic obstructive pulmonary disease (COPD)* there is a chronic obstruction to airflow due to chronic bronchitis and/or emphysema. They are two distinct processes, most often present in combination in patients with chronic airway obstruction. In *emphysema*, TLC and RV are increased, the VC is low, and the maximal expiratory flow rates are diminished. The elastic recoil properties of the lung are impaired, and in direct proportion to this impairment, the capacity of the lung to transfer CO is lowered. The elastic recoil properties of the lung serve as a major determinant of maximal expiratory flow rates. The static recoil pressure of the lung is the difference between alveolar and intrapleural pressure. During forced exhalations, when alveolar and intrapleural pressure are high, there are points in the airways at which bronchial pressure equals pleural pressure. Flow does not increase with higher pleural pressure after these points become fixed, so that the effective driving pressure between alveoli and such points is the elastic recoil pressure of the lung. Hence maximal expiratory

flow rates represent a complex and dynamic interplay between airways calibre, elastic recoil pressures, and collapsibility of airways. In *bronchitis*, TLC is often normal, and there is moderate elevation of RV. The VC is mildly diminished and maximal expiratory flow rates are invariably low. The elastic recoil properties of the lung are normal or only slightly impaired, and the capacity of the lung to transfer CO is either normal or minimally decreased.

Imaging of emphysema

The best imaging protocol for the quantification of emphysema is still an unresolved question. Due to rapidly changing CT technologies and incorporation of new imaging modalities such as MR with hyperpolarized gases, this remains an area of constant evolution.

Computed tomography (CT)

Computed tomography provides transverse anatomical images in which the value of each picture element (*i.e.* pixel) corresponds to the X-ray attenuation of a defined volume of tissue (*i.e.* voxel). The X-ray attenuation values for each set of projections (*i.e.* slice) are registered by the computer and organized in a matrix form which in today's clinical practice has a size of 512 x 512 pixels. The number of calculated pixels determines the image matrix size, influences the image resolution, and should thus be as high as possible. The X-ray attenuation, also called tissue density, is numerically expressed in Hounsfield units (HU). The scale of attenuation values range from -1000 HU, corresponding to the attenuation value of the air, to 3000 HU, 0 HU corresponds to the attenuation value of water. When alveolar walls are destructed there will be more air and less structures in the lung, and hence the HU value will be closer to that of air.

In pulmonary emphysema, the major advantage of CT is that in addition to providing data concerning overall lung destruction, it also identifies the specific locations in the lung where the alveolar structure has been destroyed. Since the late 1970s and early 1980s when emphysema detection by CT scanning was described (19, 20) many efforts have been made to improve resolution, decrease scan times, and achieve thinner collimation. CT densitometry is a potential tool for detecting the progression of emphysema but the optimal methodology is uncertain. Several technical issues remain unresolved. The level of inspiration during scan acquisition influences lung density and, in sequential studies, variability in inspiratory level will reduce the reproducibility of longitudinal data.

The technology that has been used for quantification of emphysema by many workers is the *density mask technique,* which allows highlighting of pixels in a selected range of HU (21). The pixels less than a particular value (originally -910 HU) could be

highlighted, perhaps in colour, and their number compared with the total number of pixels in the lung image. Since the original description, a lot of different parameters that could be relevant have been investigated: inspiration versus expiration, 1.5 mm versus 3 mm or 5 mm or 10 mm collimation or reconstruction, intravenous contrast material versus noncontrast, and wide (1500-2000 HU) versus narrow (800-1000 HU) windows for printing or viewing in a console. The threshold for considering a pixel as emphysematous has varied from -900 HU to -960 HU by various investigators, with various slice thickness and reconstruction algorithms. Another parameter used to measure low-attenuation regions is the *percentile point*. The nth percentile point, Perc(n) is defined as the threshold value for which n percent of all pixels have a lower density. This percentile point has been validated with pulmonary function tests (22) and pathology (23). It has been shown that the nth percentile point is equally sensitive between the 10^{th} and 20^{th} percentile, with approximately an optimum at the 12^{th} percentile (24). In practice, the 15^{th} percentile point is being used.

Several computer softwares have been developed for the analysis of the information. The one most used in Europe is Pulmo-CMS® developed in Leiden, the Netherlands by Stoel et al. (25) in collaboration with Medis medical imaging systems. The program starts by identifying the trachea, and then automatically detects the lung contours in overlapping images using a region-growing algorithm to separate lung tissue from the thoracic wall and mediastinum. Then, the information is analyzed based on the threshold chose for soft tissue-lung interface. The SPREAD study (Software Performance and Reproducibility in Emphysema Assessment: Demonstration) was established to develop a standard protocol for CT densitometry for 5 different CT scanners (25) in a multicenter study using Pulmo-CMS software. They concluded that (1) lung densitometry in a group of patients with emphysema varies mainly because of different patient lung disease status (52%), and influence of site, including differences in patients groups and scanners (47%), (2) the use of multislice-CT (MSCT) scanners would be preferable in studies on the progression of emphysema and in drug evaluation trials, and (3) recalibration for air is essential to improve the reproducibility of CT scanners and standardization between scanners, thereby reducing the intersite variation. Therefore full recalibration (for both blood and air) is recommended.

A density-mask approach alone is not sufficient to accurately distinguish normal from diseased lung (26, 27), especially in the case of early or mixed pathologic processes. The density mask is, however, particularly useful in characterizing mild/moderate and severe emphysema and has been used in the NETT (National Emphysema Treatment Trial) (28) to identify

subgroups of patients who show benefit from LVRS (lung volume reduction surgery (29)). In addition to the traditional density mask analysis Hoffman et al (30) have incorporated an additional measure, one proposed by Mishima et al. (31), which has been termed the "fractal dimensions" or "alpha". Alpha is the slope of log-log relationship of holes size versus percentage of holes at that size. The notion is that initially a random set of holes evolves in lung regions and, as such, the log-log plot of holes size versus percentage of holes is linear. However, once the initial holes have evolved, there is a greater likelihood that these holes will have destabilized the lung mechanically and the small holes will combine to form bigger holes as opposed to more small holes appearing. Thus, the slope of the log-log plot diminishes. In this way, alpha becomes an index of disease severity.

The radiation burden that CT implies is always a relevant aspect when planning longitudinal studies in patients with emphysema, because these individuals may be young and may have a favourable prognosis. A multi-detector row CT is of interest for the quantification of heterogeneously distributed emphysema, but the use of this technique increases radiation dose by as much as up to an additional 300% per examination (3.8 mSv) compared with the dose required for incremental single-detector row CT, yielding thin sections in 1-cm intervals (0.9 mSv) (32). However, Madani et al. (33) showed that using a four-channel multidetector row CT scanner the radiation dose could be reduced to 20 mAs without substantial influence on the strength of correlations between histopathological indexes and either relative areas or percentiles.

MR Imaging (MRI)

Basics

In 1952, F Bloch from Stanford University and E Purcell from Harvard University were awarded the Nobel Prize for their work on what was then known as "Nuclear Magnetic Resonance (NMR)". The method was used as a chemical analysis method. However, 20 years later with the introduction of computers in medical imaging and their capacity for calculations, the method could finally be used for imaging. The word 'Nuclear' was omitted and "Magnetic Resonance Imaging (MRI)" was introduced. In 1973, PC Lauterbur and R Damadian, working independently, pointed out the potential of the science of Magnetic Resonance in imaging the human body. Peter Mansfield of Nottingham, England, further developed the utilization of gradients in the magnetic field. He showed how the signals could be mathematically analyzed, which made it possible to develop a useful imaging technique. P Mansfield also showed how extremely fast imaging could be achievable. This became technically possible within medicine a decade later. In 2003, P Mansfield and PC Lauterbur were

awarded the Nobel Prize for their outstanding contribution in the field of Diagnostic Radiology. Since then tremendous advances have taken place in the design and technology of magnetic resonance equipment, incorporating computers and advanced software to provide sectional images of the human body with excellent delineation in the medical field. MR imaging is based on the electromagnetic activity of atomic nuclei. The human body is a chemical composition of several elements, such as hydrogen, carbon, nitrogen, sodium, etc. in various chemical combinations. It has been observed that atoms of some of these elements that have odd numbers of protons in their nuclei, possess certain magnetic properties. These properties have been utilized to produce magnetic resonance signal and images. Hydrogen (^{1}H) nuclei are used most often because of their abundance in the body, but other nuclei - for example, fluorine (^{19}F) nuclei - also may be used. In an external magnetic field the nuclei show a wobbling type of motion called "precession" and the speed with which the net magnetization vector wobbles around the magnetizing field applied is known as "precessional frequency" which is expressed in megahertz (MHz). The precessional frequency is often called the "Larmor's frequency" and it is directly proportional to the strength of the magnetic field. When a patient is placed in the strong magnetic field in the MRI scanner, a certain amount of the hydrogen nuclei in the body align with the applied external magnetic field building up a net magnetization vector along the magnetic field. When exposed to a short burst of electromagnetic energy in the form of radiofrequency (RF) pulses with a frequency that equals the Larmor´s frequency the nuclei in the patient's body absorb this energy which changes the direction of the magnetic vector. When the RF pulse is finished the vector flips back to the aligned position in the external magnetic field. During this process (relaxation) a signal is sent out which can be detected. This process is known as 'magnetic resonance'. It forms the basis of MR imaging. The MR signals obtained have a wide range of specificities, depending on the strength of the magnetic field, the frequency and duration of radiofrequency waves and the magnetic gradients employed (pulse sequence), the proton density, the element containing the protons, the chemical combination of elements, their molecular state, etc. The magnetic resonance signals have specific tissue characteristics. In MRI the signals are analyzed by a computer and reconstructed mathematically by a process known as "Fourier transformation" into sectional images of the human body.

There are two key parameters in the creation of image contrast, repetition time (TR) and echo time (TE). TR is the time (usually measured in milliseconds) between the application of an RF excitation pulse and the start of the next RF pulse (34, 35). TE is the time (also

usually measured in milliseconds) between the application of the RF pulse and the peak of the echo detected (34, 35). Both parameters affect contrast on MR images because they provide varying levels of sensitivity to differences in T1 and T2 relaxation times between various tissues.

In order to detect which tissue the signal is coming from, magnetic field gradients are employed in MRI systems. Gradients are linear spatial variations of the magnetic field strength in a selected region (36). Three perpendicular gradients are applied in MRI. The section-selective gradient selects the section to be imaged. The phase-encoding gradient causes a phase shift in the spinning protons so that the MR imaging system computer can detect and encode the phase of the spin. The frequency-encoding gradient also causes a shift - one of frequency rather than phase. Both help the MR system to detect the location of the spinning nuclei. The resulting set of signals is stored in k-space from which the MR-system computes the exact location and amplitude of the signal (37). The centre of K-space contains information about gross form and tissue contrast, whereas the edges (periphery) of k-space contain information about spatial resolution (details and fine structures).

There are two fundamental types of MR pulse sequences: spin-echo (SE) and gradient-echo (GRE). All other MR sequences are variations of these, with different parameters added on. Among SE-based sequences are: fast SE variants, conventional inversion recovery, STIR and FLAIR. Among GRE sequences are: partially refocused GRE, fully refocused GRE and spoiled GRE. However, there are also types of imaging sequences that can use both spin and gradient echoes, echo-planar imaging and diffusion-weighted imaging. With *echo-planar imaging*, a single echo-train is used to collect data from all lines of k-space during one TR. This technique shortens the acquisition time substantially (38). *Diffusion weighted (*DWI) enables one to distinguish between rapid diffusion of protons (unrestricted diffusion) and slow diffusion of protons (restricted diffusion) (39). DWI has mainly been used in the diagnosis of stroke. The basic principle of diffusion imaging is that the small random motion of the molecules results in a Gaussian distribution of phases. The strength and duration of the diffusion gradients and the direction in which they are applied influence the sensitivity to different length scales. Diffusion-weighted sequences are usually applied in conjunction with apparent diffusion coefficient (ADC) mapping techniques. For the calculation of ADC maps, two sets of images are required: one set obtained without application of a diffusion gradient, and one obtained with a diffusion gradient. The ADC calculation is based on the negative logarithm of the ratio of those two image sets.

MRI is an imaging technique that has proven to be extremely valuable in

the medical assessment of many body regions. A notable exception has been the lungs as due to the low proton concentration in air, ^{1}H-MRI does not visualise aerated spaces within the body. Normal lungs consist mainly of aerated spaces and, consequently, have very low magnetic resonance signal. Its complicated three-dimensional structure of tissue and ventilation, with many air-tissue interfaces, magnetic susceptibility gradients, also produces artefacts in conventional MR images (40). Potential approaches to resolve the signal intensity problem in the lungs can be derived from a consideration of some of the controllable factors that determine signal intensity. The extent of magnetic polarisation (i.e. the fraction of nuclei in each orientation) is determined by the temperature and by the difference in magnetic energy between the high and low energy orientations (which is determined by the magnetic properties of the nuclei and by the strength of the external magnetic field). For protons undergoing MRI at 1.5 Tesla, the degree of polarisation is quite low, in the order of 1 x 10^{-4}%. The degree of polarisation is one major determinant of signal intensity during MRI, and another factor is the concentration of nuclei. The degree of polarisation can be affected directly by lowering the temperature (not feasible in vivo), or by increasing magnetic field strength (which has practical limits). But even if these were feasible, there would still remain the problem of low proton concentration in the lungs.

One possible approach to solving the problem would be to find a more efficient way to polarize nuclei. Such a method is the *hyperpolarisation* of certain isotopes of noble gases.

Hyperpolarisation process

Hyperpolarisation involves polarising nuclei before MRI; using methods that can give levels of nuclear polarisation that are up to 10^{5} times higher than those achievable during conventional MRI. Of particular interest for hyperpolarized (HP)-gas studies of the lungs are the two nonradioactive noble-gas isotopes, ^{3}He and ^{129}Xe.

^{3}He is produced from the nuclear decay of tritium and the total amount on earth is only ~ 200 kg (41) while large quantities are available on the moon, resulting from the nuclear fusion process within the sun (42). This makes ^{3}He relatively expensive. However, ^{3}He has 2.8 times larger gyromagnetic ratio (and hence magnetic moment determines the signal-to-noise ratio – SNR - than ^{129}Xe, resulting in better image quality. Besides, no systemic adverse effects have been observed due to the negligible uptake in blood, making this gas safe when inhaled in large quantities. On the other hand, ^{129}Xe is relative abundant in nature (~26%) and thus less expensive. However, it is highly soluble in biological tissues and undesired events such as euphoric and anaesthetic effects have been reported (43, 44). Besides, due to the lower gyromagnetic ratio of ^{129}Xe, the SNR is expected to be ~10

times lower than ^{3}He at the same experimental conditions. One way to avoid this matter is enrichment of the isotope to 70%-80% but this process is relatively expensive. With regard to the level of polarisation, the practical limit for both gases is between 50 and 100 percent and depends on the polarisation technique.

Three techniques have been employed to produce HP noble gases to date. The two most used techniques, optical pumping spin exchange (OPSE) and metastability exchange (ME), employ the direct transfer of angular momentum from optical photons to nuclei to enhance polarisation. The third technique is an extreme extension of thermal-equilibrium polarization and is less used. While the three techniques merit detailed discussions, the present work will focus on the OPSE which was the technique we employed.

A mixture of ^{3}He and N_2 gases (ca. 1.1 to 1.2 L at room temperature and atmospheric pressure) and ca. 1 ppm of Rb metal in the gas phase at 8-10 atm pressure in a ca. 0.15 L glass bulb is placed in a magnetic field and heated to approximately 160°C, at which temperature a very small amount of the rubidium is in the vapour phase. Rubidium has an unpaired electron which has a magnetic moment and which can therefore adopt 2 different orientations (parallel or antiparallel) with respect to an external magnetic field (analogous to the behaviour of ^{1}H atoms during MRI). A high-power diode laser tuned to the 795 nm, D_1 resonance of Rb illuminates the bulb with circularly polarised light, which induces electronic magnetic polarisation of the unpaired electron in the Rb atoms. A gas-phase collision between an electronically magnetically polarised Rb atom and an unpolarised ^{3}He atom allows the transfer of the electronic orientation to the nuclear spin at the ^{3}He-atom. During the collisional spin exchange process, the level of polarisation increases until a steady state is reached, at which point the rate of ^{3}He polarisation equals the rate of ^{3}He depolarisation. Levels of polarisation up to at least 30% (containing a final concentration of ^{3}He with a net activity of 12 mmol/L) are achievable using this method. The degree of polarisation can be monitored during the hyperpolarisation process. After the desired level of polarisation is reached, the glass bulb is allowed to cool to room temperature and the Rb vapour condenses onto the wall of the glass bulb. To remove any potential contamination of the ^{3}He gas with any remaining Rb, the gas is passed trough a 0.003 μm filter (Wafergard GT Plus In-Line Gas Filter, manufactured by Millipore). The method provides a T1 relaxation time of about 24 hours. The administration bag, which will be used to deliver the gas to the subject, provides a T1 relaxation time of at least 3-4 hours. After one T1 the polarisation has decreased to 0.37 of its starting level. Upon inhalation, HP ^{3}He in the lungs may undergo depolarisation because of residual oxygen, which is

paramagnetic and therefore can induce shortening in T1. The T1 in lungs has been calculated to be 26 seconds (45). In addition, HP ^{3}He depolarises during MR-examination as magnetisation is consumed by the MR sequence. The degree of depolarisation depends on the imaging parameters. After MR imaging, hyperpolarisation may only be restored by separating ^{3}He from the exhaled gas mixture and going through another optical pumping process.

Albert et al in 1994 (46) demonstrated the first MR images of excised mouse lungs filled with HP-^{129}Xe, and a few years later Mugler et al (47) showed the first image of human lungs, obtained from healthy volunteers, also with HP- ^{129}Xe, followed by Bachert et al, Ebert et al and MacFall et al (48-50) who showed human lung images using ^{3}He. Since then HP MRI has shown a rapid development to the present variety of functional imaging techniques.

The development of HP ^{3}He MRI technique has led to four principal applications in human subject studies: *Static Ventilation Imaging (Spin Density)* to see areas that are better ventilated than others and perform volume measures. This technique usually use a 2D multislice, spoiled gradient-recalled echo (SPGR) sequence with low flip angle RF pulses (7-10°) and short TE. Ventilation measures correlate well with FEV_1 in obstructive lung diseases (51, 52) and with regions of decreased parenchymal density on CT for patients and smokers with COPD and bronchiolitis obliterans (BO) syndrome in lung transplants (53, 54). However, more work is needed to quantify the gradations of signal density to true quantitative ventilation. *Dynamic Ventilation Imaging* gives information of the respiratory cycle and improves the information from traditional lung function tests by providing quantitative measures of airflow on a regional basis (55, 56). It is based on ultrafast pulse sequences such as GRE or EPI and more recently with the increasing application of parallel imaging the acquisition speed can be accelerated even more. Qualitative measurements of gas trapping have been demonstrated in asthma (51) and cystic fibrosis (57). *Regional Ventilation to Perfusion Ratio* (V_A/Q) to assess ventilation and perfusion uses the paramagnetic effect of oxygen on the depolarization of ^{3}He. Eberle et al (58) have shown that after correction for RF-pulse effects the oxygen-induced signal decay rate is linearly proportional to the concentration of oxygen. The regional PO_2 can be used to deduce V_A/Q using mass-balance relationships for alveolar CO_2 and O_2 gas exchange. This information has been used experimentally (59) to assess ventilation and perfusion response in asthma as well as the mismatch in V_A/Q observed in pulmonary embolism and in BO of lung transplant. *Diffusion Weighted Imaging (DWI)* to assess lung microstructure, measures the apparent diffusion coefficient (ADC) of the HP gas within the lung airspaces. The high

self-diffusion property of ^{3}He (approximately 2 cm^2/s at body temperature and a pressure of 760 Torr) is used, as in the lungs diffusion becomes effectively restricted by the boundaries of the air spaces. Thus, in regions such as the trachea, the gas is largely unrestricted, but in the lung parenchyma, the gas is highly restricted by the walls of the alveoli and terminal bronchioles. This gas behaviour is of especial interest in diseases such as emphysema in which alveoli are enlarged, the gas is less restricted and can diffuse over greater lengths resulting in greater signal loss. Thus, the ADC is increased and this enables an indirect measurement of the movement of the ^{3}He atoms within a restrictive environment and thereby an estimation of the size of the alveoli. The ADC measurement is typically depicted as an ADC map and histogram of ADC values (Fig 2). The method which has been used in the majority of the studies is a gradient-echo pulse sequence modified by the addition of a bipolar diffusion-sensitizing gradient waveform between the excitation RF pulse and the data acquisition (60-63). Fast spin-echo pulse sequences (64) and magnetic-tag dissolution (65) have also been used and seem to be more sensitive to gas diffusion over longer length scales. Assuming the diffusion coefficient of ^{3}He mixed with air in the lungs is taken to be $D_0 = 0.86$ cm^2/s (60), it is possible to probe different length scales using the DW sequences by changing the pulse delays. Values for length scale in the different studies have vary from ~0.5 mm (62, 63, 66) to several centimetres (65, 67) and more recently Mugler et al.(68) showed that the ADC remains dependent on diffusion time for times up to at least approximately 10 seconds when different length scales were used. The monoexponential model for signal decay has been used for most studies providing regional information, but it is now recognized that a multiexponential model for signal decay probably should be used. This is most likely due to multiple scales of restricted diffusion within the lungs (66, 69, 70). Thus, future investigations could incorporate multiple b-value measurements using modified spin-echo pulse sequences (71) or diffusion tensor imaging combined with modelling (66).

HP ^{3}He-diffusion MRI technique has developed rapidly in a short time and several studies have showed the sensitivity of this technique to lung changes in COPD. There are still no standard ADC normal values for lungs at different ages; mean ADC value vary among different researches from 0.17 to 0.28 cm^2/s which is quite wide range. There are also no standardized measurement techniques, since different research groups use different coils, MRI scanners, field strength, and pulse sequences. It is fundamental for clinical studies that the measurement precision is evaluated to permit quantitative comparison of ADC among research groups and over time. In this way it is possible to understand the variability which can be attributed to those above

mentioned related to the scanner, those related to the subject (breath-hold, motion), and those related to the methodology used including gas delivery and the way to analyze the data. Potential physiologic and radiologic changes that occur over short and long periods are of high interest from a clinical point of view, as well as from a drug development point of view where the purpose is to evaluate the effect of newly developed drug therapies in as short time span and as small patient group as possible. All of these factors made it important to try to validate the method in order to show the short- and long-term reproducibility, to compare the method to accepted standard methods (CT and PFTs) and try to demonstrate disease progression.

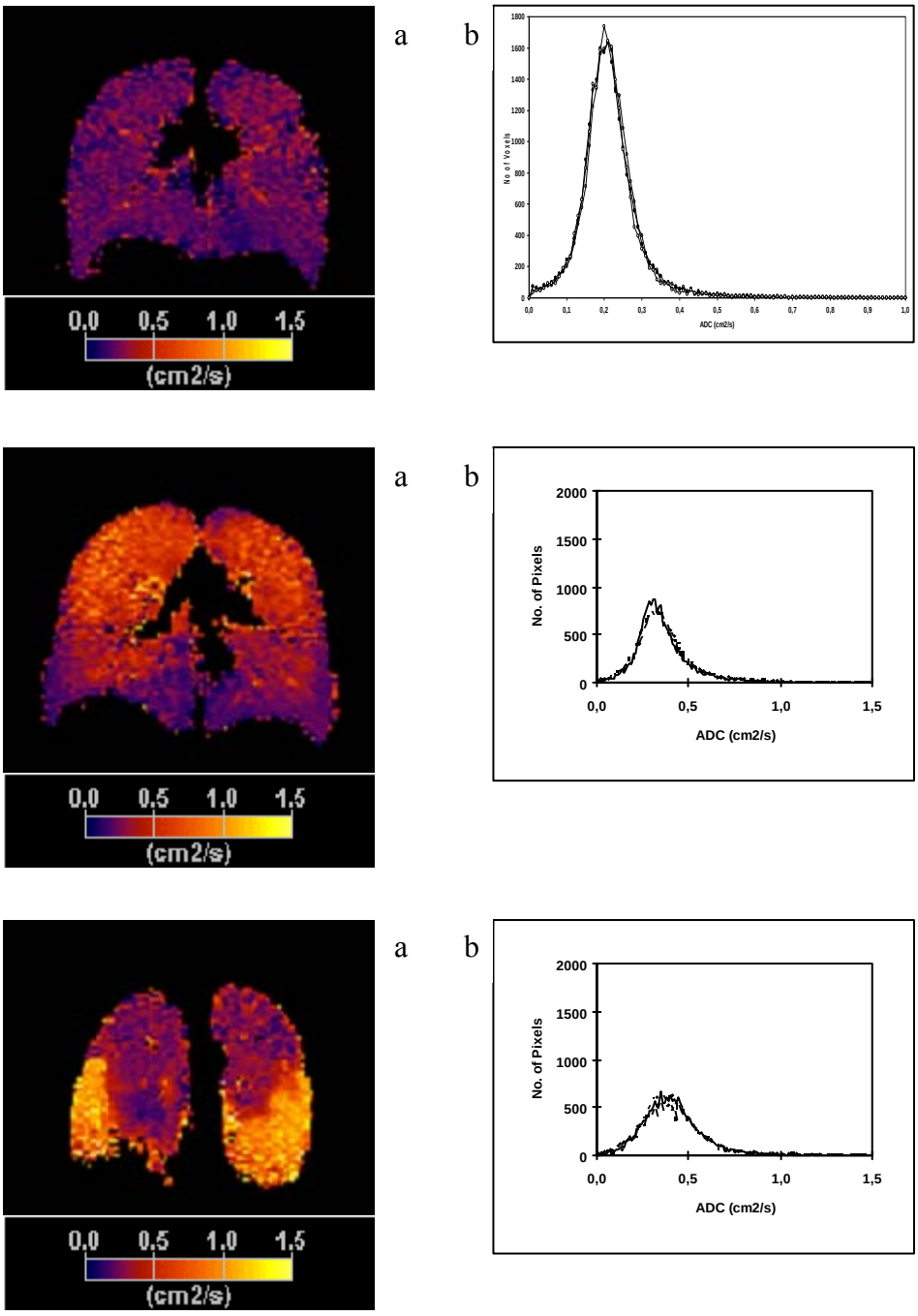

Fig 2: Upper row: Healthy volunteer a) ADC-map, b) histogram.
Middle row: COPD a) ADC-map, b) histogram.
Lower row: AAT (alpha-1-antitrypsin deficiency) a) ADC-map, b) histogram

AIMS OF THE STUDY

The general aim of this work was to evaluate the potential of hyperpolarized ^{3}He-diffusion MRI technique to diagnose early emphysema changes in the lungs.

In the different papers the specific aims were:

I. To assess the values and the reproducibility of the ADC measurement in volunteers and patients with mild to moderate emphysema, to study the dependency of the ADC on inhaled volume of gas, and to confirm any gravity effect.

II. To determine the long-term reproducibility of the ADC in healthy volunteers, to analyze if any age-dependency of ADC exists and to assess if an anatomical variation of ADC exits in the lungs.

III. To assess the emphysematous enlargement of distal airspaces in patients with emphysema with hyper-polarized helium MRI technique and to compare results with multislice CT (MSCT) and pulmonary function tests (PFT) as an approach to validate this new imaging modality.

IV. To evaluate if mean ADC value from hyperpolarized ^{3}He- diffusion MR technique is sensitive enough to detect emphysema progression over 12 months or if other, more sophisticated methods or analyses should be used.

MATERIALS, METHODS AND RESULTS

Subjects

All studies were conducted in full accordance with the current revision of the Declaration of Helsinki, the Good Clinical Practice, Consolidated Guideline approved by the International Conference on Harmonization (ICH), and with the approval of the local ethics committee at Lund University or the regional ethics committee in Lund. Written and oral information was given to all subjects. Written informed consent was obtained from each subject before any procedures or assessments were done and after the aims, methods, anticipated benefits, and potential hazards were explained.

Screening of subjects to determine whether they met all of the inclusion criteria and none of the exclusion criteria was performed between 7 days to 24 hours before image session. Demographic information (age, gender and race), body measurements (height, weight), medical history and/or prior (occupational) exposure to any specific air pollutants (e.g., asbestos, coal dust, quartz dust, etc.) was obtained and recorded.

In addition, subjects underwent the following assessment including:

- Medical and surgical history.
- Limited physical examination, including limited neurological examination.
- Vital signs (blood pressure, heart rate, respiratory rate, and body temperature)
- SaO_2 (oxygen saturation)
- Clinical laboratory tests (haematology, biochemistry, and urine analysis).
- 12-Lead ECG (PR, QRS, QT, QTc, and RR)
- For women of childbearing potential, a urine dipstick pregnancy test was performed.
- Concomitant medications.
- Spirometry acquired with the subject in a sitting position before and after administration of 2 puffs of albuterol from a metered-dose inhaler (MDI). The date and time, and the results and percent of predicted normal values at baseline was recorded (FEV_1, FEV_1/FVC, FVC, $FEF_{25-75\%}$, PEF).
- Body plethysmography was performed after FEV_1 reversibility test. The date and time, and the results, as well as normal ranges were recorded (FRC, TLC, sRaw, sGaw).
- Diffusing capacity of carbon monoxide-single breath ($D_{L,CO}$-SB) was measured.

FEV_1 Reversibility

A FEV_1 test was performed before and after administration of 2 puffs of albuterol from a MDI. An increase of <12% in FEV_1 following albuterol administration was required. The post bronchodilator FEV_1 test was performed between 15 minutes and 1 hour post albuterol administration.

MRI examination

Prior to ^{3}He-MRI, a proton MRI of the lungs was acquired to provide anatomical localization of the lungs. The subjects were asked to inhale 500 mL of room air from a bag at FRC. Approximately 5 minutes before the first ^{3}He imaging during each imaging day, subjects were asked to inhale a portion (sip) of ^{3}He from a bag with approximately 30 mL of polarised ^{3}He plus approximately 970 mL of N_2 to allow adjustment of the MR scanner to the ^{3}He frequency. This was followed by inhalation of the rest contents of the bag to adjust transmitter gain.

Polarization of the ^{3}He gas was performed with a prototype polarizer (IGI.9600.He, GE Healthcare, Durham, NC, USA) which used the method of collisional spin exchange between laser-polarized rubidium vapour and ^{3}He (72). The polarized ^{3}He gas with a net activity (defined as the number of mmoles of helium-3 atoms that have been polarized) level of 3.5 to 4.5 mmol was dispensed into 1-2 litre Tedlar bags (Jensen Inert, Coral Springs, FL, USA) and mixed with nitrogen (N_2).

MR imaging was performed using a 1.5 T whole body MR scanner (Siemens Magnetom Sonata; software: syngo MR 2002 B; Siemens Medical Solutions, Erlangen, Germany). A diffusion-weighted 2D gradient-echo sequence (helium body coil, TR/TE 9.6/5.9 ms, flip angle 7°, bandwidth 250 Hz/pixel, field of view (FOV) 382x470 mm, matrix 80x128, coronal slice direction, slice thickness 15 mm, inter-slice distance 5 mm, number of slices 10, time of acquisition 15 sec) was used for hyperpolarized ^{3}He ADC MR imaging. Two images were acquired at each slice position, one without (b0) and one with (b1) a bipolar diffusion-sensitizing gradient waveform (b0=0 s/cm^2, b1=1.6 s/cm^2) applied in the slice direction with interleaved phase encoding. The coronal slices covered the whole lungs from anterior to posterior. The b0 images were used as ventilation images. A flexible quadrature vest coil (Clinical MR Solutions, LLC, USA) was used for all ^{3}He scanning. The Helispin™ Workstation software (GE Healthcare) was used for post-processing. An ADC map was calculated from each pair of b0- and b1-images on a pixel-by-pixel basis. A linear least square fit to the natural log of the signal amplitude versus the b-value was applied. Background pixels were excluded from the ADC calculation using a threshold of 5 times the true standard deviation (SD) in a background region. This SD was obtained by dividing the background mean by 1.253 (73, 74). To eliminate bias from ADC calculated in the large airways, the trachea and main bronchi were manually segmented from the ADC-maps before analysis by a radiologist. ADC maps and frequency distributions (No. of voxels versus ADC values) were calculated for individual slices and the whole lungs. The mean ADC and the SD were computed from the ADC-map of all individual slices covering the whole lungs.

Paper I

Hyperpolarized ^{3}He Apparent Diffusion Coefficient MRI of the Lung: Reproducibility and Volume Dependency in Healthy Volunteers and Patients with Emphysema

Material and methods

Subjects

Two different populations were included: one group of 8 healthy volunteers (3 men, 5 women; age range 40-60 years) with normal physical examination results, no smoking during the last five years and no more than a 5 pack-year smoking history, pulmonary function test with FEV_1 > 80% of predicted normal value and FEV_1 /FVC >70%. The patient group, in total 16 patients, consisted of 2 subgroups: eight patients with emphysema due to alpha-1 antitrypsin deficiency (AATD), phenotype PiZ (5 men, 3 women; age range 30-70 years), with FEV_1 50% to 80% of predicted normal value and FEV_1 /FVC < 70% and eight patients with usual COPD emphysema phenotype PiM (2 men, 6 women; age range 40-60 years) with FEV_1 50% to 70% of predicted normal values and FEV_1 /FVC < 70%.

All subjects underwent PFT performed according to the Guidelines of the European Respiratory Society (75). The inclusion criteria were followed strictly and patients with mild to moderate emphysema could thereby be enrolled.

Each subject was imaged on 3 separate days during a 7-day period and received two volumes of HP ^{3}He during on each of the three imaging days with one volume being 6% and the other 15% of TLC. All volumes had a planned net concentration of 4.5 mmol-hyperpolarized ^{3}He but different volumes of filler gas (N_2). The gas was administered in the supine position by instruction the subject to inhale from functional residual capacity (FRC) until the bag was empty.

Statistical analysis

Statistical analysis was performed using SAS® software. The results from the mean ADC measurements across all lung slices for each subject, day and volume inhaled were analyzed using a mixed model repeated-measures analysis of variance. This mixed model utilized subjects as a random effect and day, volume and day-by-volume interaction as fixed effects. The volume (6% and 15%) administered was calculated as a percentage of TLC for each subject. The analysis was used to test for an overall difference among the volume, day, and volume-by-day interaction. The interaction term indicated the reproducibility of the

administration of each given volume over time. Assuming no significant interaction existed; simultaneous 95% confidence intervals were constructed on adjusted mean of ADC by imaging day and on all pair wise differences of the mean ADC between imaging day across volumes.

Results

Healthy volunteers could be clearly discriminated from patients. The findings at 15% of TLC are shown in Fig 1.

The overall mean ADC in each subject (mean value of three measurements) at both volumes showed a small intra-individual difference with low SD for all subjects (healthy volunteers SD range was 0.003-0.013 cm^2/s and 0.001-0.009 cm^2/s at 6% and 15% of TLC, patients SD-range was 0.001-0.041 cm^2/s and 0.001-0.011 cm^2/s at 6% and 15% of TLC).

The inter-individual difference in overall mean ADC per subject among the healthy volunteers was small [range 0.184 to 0.234 cm^2/sec (inter-individual SD 0.020) and range 0.193 to 0.247 cm^2/sec (inter-individual SD 0.021) both at 6% and 15% of TLC].

The mixed model analysis (dependence of mean ADC on day, volume and day-by-volume) showed no statistically significant day or day-by-volume effects on the overall mean ADC and SD per subject but showed significant dependence of the volume in both patients (p-value 0.027) and healthy volunteers (p-value 0.001) (Table 1).

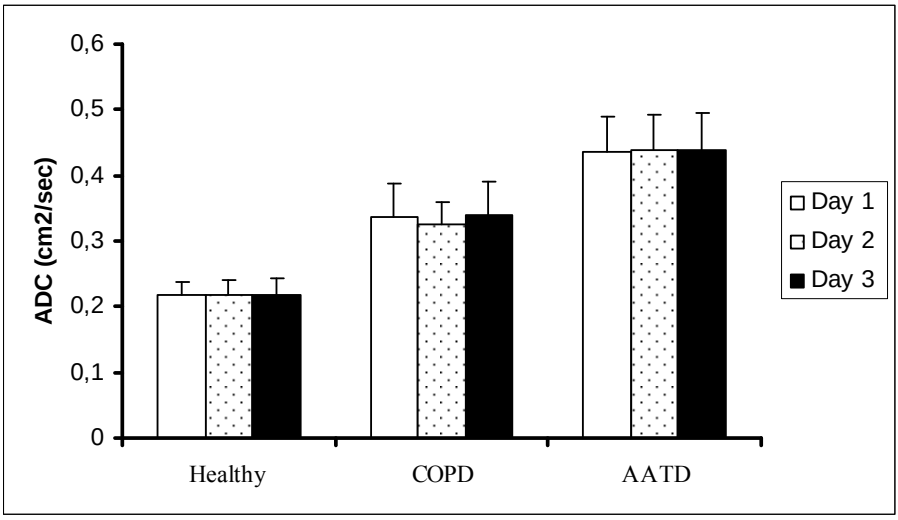

Figure 1. *Group Mean ADC at each imaging day at the larger volume (15% of TLC) for all subjects in each group. The error bars represent the standard deviation of the three measurements on three separate days. Note the clear discrimination between the healthy volunteers and the patients.*

Table 1. *Results of the mixed model analysis of overall mean ADC and SD.*

		Mean ADC*		SD* ADC	
	Effect	F-value	p-value	F-value	p-value
Emphysema group	Day	0.94	0.403	0.41	0.669
	Volume	6.26	0.027	3.96	0.068
	Day x Volume	1.63	0.216	0.10	0.905
Healthy group	Day	1.91	0.185	2.71	0.102
	Volume	26.20	0.001	19.35	0.003
	Day x Volume	1.27	0.312	1.52	0.252

**ADC: apparent diffusion coefficient. SD: standard deviation.*

In healthy volunteers an anterior-posterior ADC gradient was found (Table 2). In the supine position the mean ADC was higher in anterior than posterior slices with a mean change of 31.1±7.9% at the 15% dose.

Table 2. *Anterior-posterior mean ADC at 15% of total lung capacity (TLC)*

Healthy subjects	Anterior slices (mean ADC)	Posterior slices (mean ADC)	Gradient
1	0.224	0.173	0.051
2	0.262	0.195	0.067
3	0.207	0.171	0.036
4	0.264	0.196	0.068
5	0.224	0.179	0.045
6	0.247	0.202	0.045
7	0.242	0.178	0.064
8	0.304	0.210	0.094
Group	0.247	0.188	0.059

Paper II

MR Imaging of Hyperpolarized Helium in Healthy Subjects: Long-term Reproducibility, Age-dependency and Anatomical Variations

Material and methods

Subjects

A total of 16 healthy non-smoking volunteers (6 women and 10 men; age range 25-73 years) were included. Inclusion criteria were: FEV_1 and $D_{L,CO}$ >80% of predicted normal values, FEV_1/FVC >70%, O_2 saturation >90%.

At all imaging sessions each subject received two identical volumes of gas, each equivalent to 15% of TLC. Imaging was performed at 0, 6 and 12 months.

Data analysis

The data were analyzed to show the long-term reproducibility of mean ADC in healthy subjects; to detect regional variation of mean ADC in the lungs, and to detect dependency between age and mean ADC.

1. Long-term reproducibility data were analyzed using SAS® software. Changes in ADC measurements (mean and SD of ADC across all lung slices for each subject) were examined versus time (imaging day) using a mixed repeated measures analysis of variance model. The volume-by-day interaction term indicated the reproducibility of the administration of single volume over the time. Confidence intervals of 95% were constructed.

2. The anatomical variation of mean ADC in the lungs was analyzed in different ways: anterior *vs.* posterior and apical *vs.* basal. The *anterior-posterior* difference was calculated as the absolute difference of mean ADC per slice between the most anterior slices, using the trachea as a landmark, and the most posterior slices of both lungs. Mean ADC of the whole slice with exclusion of the trachea and main bronchi was used. A paired t-test was performed. The *apical-basal* variation was analyzed as follows: The four most central coronal slices were selected. The trachea and main bronchi were manually segmented and these ADC values were excluded from further analysis. A small region of interest (ROI) was placed in the most upper and lower regions of the lung of each selected slice by a single training radiologist. The ROIs were selected to avoid bias in deriving mean ADC due to the larger airways in the middle region of the lungs. Mean ADC was calculated for each coronal slice and for each of the superior and inferior ROIs of both the right and the left lung. The absolute difference for superior and inferior ROIs of both lungs was calculated and a paired t-test was performed.

3. The age-dependency of mean ADC, was analyzed using a non-parametric correlation test. Spearman's Rho was used to analyze the association between the mean ADC values of the whole lungs and the age of the participants. A linear regression analysis was used to calculate the relationship between age and mean ADC of the different regions of the lung.

Results

1. Long-term reproducibility analysis

A total of 16 subjects were included but 4 of them were examined only once due to personal reasons. Data from 12 healthy volunteers were analyzed, 11 subjects examined three times (0, 6 and 12 months). One volunteer did not complete the 12-month examination due to technical problems. The mean ADC values of the whole lungs were reproducible between the examination days (Figure 1). The SD of the intra-individual mean ADC ranged between 0.002 and 0.013. Mean ADC ranged between 0.158 and 0.298 cm^2/s.

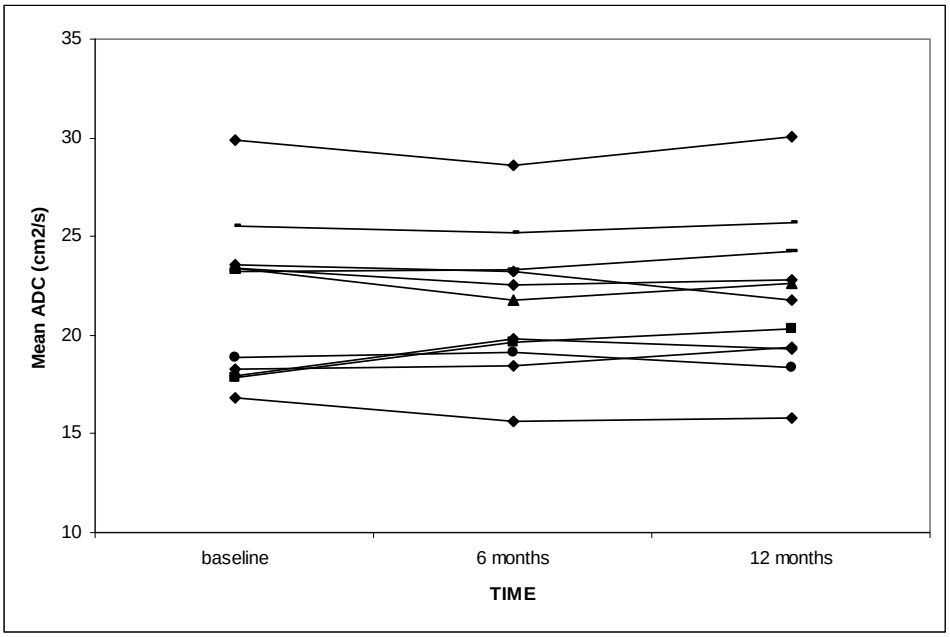

Figure 1. *Long-term reproducibility of Mean ADC (cm^2/s) for each subject at three measurement points*

2. Anatomical variation of ^{3}He-ADC in the lungs

The analysis used the baseline results and included all 16 participants. Mean ADC was higher in the anterior slices than in the posterior slices. The mean anterior-posterior difference was 0.034 (p=0.0001) (Table 1). The group variation of mean apical ADC and mean basal ADC of the lungs was not significant (p=0.8769).

Table 1. *Mean ADC anterior-posterior difference. The gradient was calculated as the absolute difference of mean ADC per slice between the most anterior slices and the most posterior slices of both lungs.*

	Mean ADC (cm^2/s)		Difference (cm^2/s)
Subjects	Anterior	Posterior	
1	0.312	0.257	0.055
2	0.210	0.196	0.014
3	0.247	0.186	0.061
4	0.201	0.193	0.008
5	0.185	0.143	0.042
6	0.194	0.171	0.023
7	0.243	0.203	0.04
8	0.261	0.258	0.003
9	0.256	0.216	0.04
10	0.191	0.182	0.009
11	0.251	0.225	0.026
12	0.231	0.185	0.046
13	0.224	0.173	0.051
14	0.207	0.171	0.036
15	0.242	0.178	0.064
16	0.304	0.210	0.094
Mean	0.230	0.204	0.038
SD	0.034	0.031	0.024

3. Age-dependency of mean ADC

The analysis used the baseline results and included all 16 participants. The Spearman's Rho correlation analysis showed significant correlation between mean ADC and age, r = 0.58; p = 0.017 with a 95% confidence interval 0.0035 to 0.0030 (Fig 2). The correlation between ADC and age in the different regions of the lung was slightly higher in the apical regions of the lung (r=0.65; p=0.005) than in the basal regions (r=0.55; p=0.025).

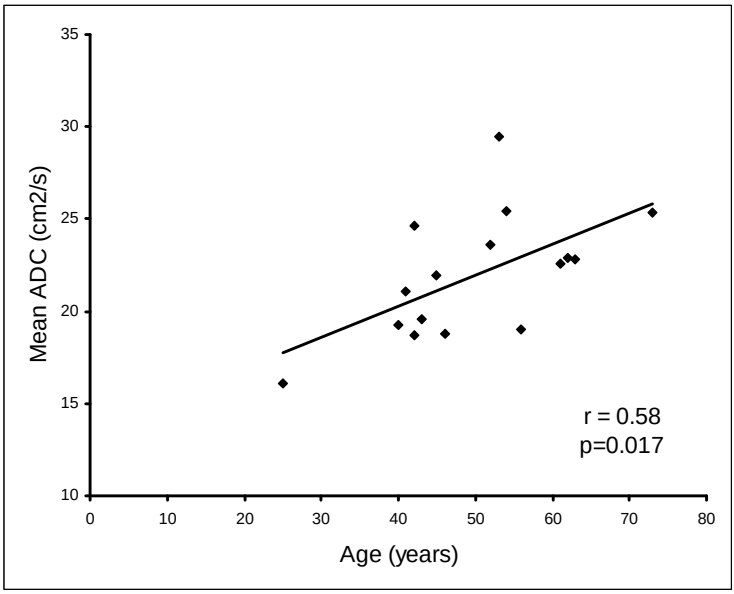

Figure 2. *Age dependency of Mean ADC (cm^2/s). The analysis shows a positive correlation between mean ADC and age, r = 0.58; p = 0.017 with confidence interval 0.0035 to 0.0030.*

Paper III

Validity of Apparent Diffusion Coefficient Hyperpolarized ^{3}He-MRI using MSCT and Pulmonary Function Tests as References

Material and methods

Subjects

The study included 27 subjects (9 men, 18 women; age range 25-75 years). The subjects were divided in two groups: established emphysema and pre-clinical emphysema. The established emphysema group included 22 subjects, 18 with usual COPD (9 currently smoking subjects and 9 ex-smoking) and 4 with the homozygous form of alpha-1-antitrypsin (AAT) deficiency (PiZZ). The inclusion criteria were: FEV_1/FVC <70%, $D_{L,CO}$ <70% and FEV_1 between 40 and 70% of predicted normal values. The pre-clinical emphysema group included 5 subjects with the homozygous form of AAT with PFT as follows: FEV_1/FVC >70%, $D_{L,CO}$ <85% and FEV_1 >80% of predicted normal values.

Each subject received 2 identical volumes of HP ^{3}He with a net activity of 3.5 to 4.5 mmol. Imaging was done at FRC + 15 % of the TLC.

CT Examination

Non-enhanced low dose MSCT examination of the whole lungs was performed within 45 days of the MRI at full inspiratory breath-hold (i.e., TLC) after three deep inhalation manoeuvres (effective mAs 20, kV 120, scan time 7.06 sec, delay 5 sec, slice thickness 5 mm, rotation time 0.5 sec, pitch 1.5, reconstruction filter B10f (very smooth), FOV 300 mm and acquisition in caudal-cranial direction). Emphysema Index (EI), 15th percentile and Mean Lung Density (MLD) of the whole lungs were calculated using Pulmo-CMS software. EI was defined as the ratio of the number of voxels with Hounsfield Units (HU) less than -950 over the number of voxels with HU over -950. MLD was defined as the average of the total lung density of all patients.

Statistical analysis

Data analysis and statistics were performed using Microsoft Office Excel 2003® (Microsoft Cooperation, Redmond, Washington) and SPSS 9.0.1® (SPSS Inc., Chicago, IL). Statistical tests were determined to be significant at α=0.05 level and confidence intervals were calculated at a 95% level of confidence. Linear least squares regression lines and Pearson correlation coefficients between different PFTs (% predicted $D_{L,CO}$, % predicted FEV_1, FEV_1/FVC, EI, 15th

percentile, MLD and mean ADC values were calculated.

Results

Group mean of the mean ADC differed between groups; 0.392 cm^2/s ± 0.119 for established emphysema and 0.216 cm^2/s ± 0.046 for pre-clinical emphysema. Group mean EI differed; 11% ± 12 for established emphysema and 0 % ± 1 for pre-clinical emphysema. The group mean of the 15th percentile was -956 HU ± 25 versus -933 HU ± 14 and the group mean MLD was -877 HU ± 20 versus -863 HU ± 15.

Good correlations (in each patient) between mean ADC from HP ^{3}He MRI and EI and 15th percentile from MSCT were found with r = 0.90 and r = -0.90 (Figure 1 and 2).

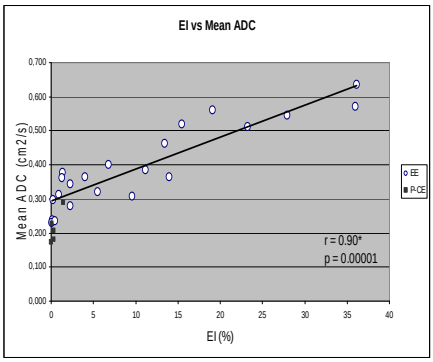

Figure 1. *Graph showing the correlation (r = 0.90) between mean ADC (apparent diffusion coefficient) from ^{3}He- MRI and EI (emphysema index) from MSCT. *The correlation is significant at the 0.01 level (two-tailed). The circles represent patients with established emphysema and the squares patients with pre-clinical emphysema. The established emphysema group shows higher ADC values with higher EI while the pre-clinical emphysema group shows lower ADC values (normal) with EI values near to zero.*

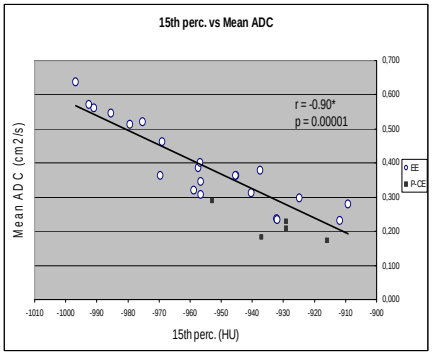

Figure 2. *Graph showing the negative correlation (r = -0.90) between 15th percentile point in HU (Hounsfield Units) from MSCT and mean ADC (apparent diffusion coefficient) from ^{3}He-MRI. *The correlation is significant at the 0.01 level (two-tailed). The circles represent patients with established emphysema and the squares patients with pre-clinical emphysema. The negative correlation is very close for both groups.*

The correlation between mean ADC and MLD was lower (r = -0.59) than with the other parameters from MSCT (Figure 3).

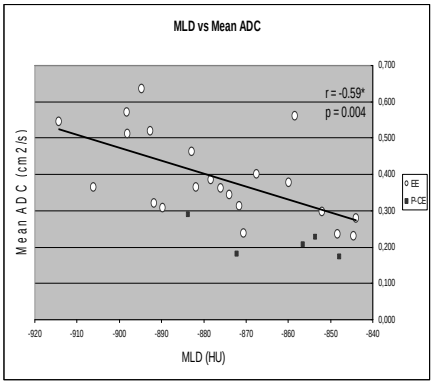

Figure 3. *Graph showing the negative correlation (r = -0.59) between mean ADC (apparent diffusion coefficient) and MLD (mean lung density). *The correlation is significant at the 0.01 level (two-tailed). The circles represent patients with established emphysema and the squares patients with pre-clinical emphysema. The higher ADC values in the patients with emphysema do not correspond well with lower lung density values. The pre-clinical group shows lower ADC and MLD values.*

Percent predicted $D_{L,CO}$ showed higher correlation with mean ADC (r = 0.82 Figure 4) than with EI and 15th percentile (0.66 and 0.60 respectively Figures 5 and 6). There was no correlation between % predicted $D_{L,CO}$ and MLD (r = 0.29, data not shown). The correlations with % predicted FEV_1 and FEV_1/FVC were slightly lower, but better with mean ADC than EI (r = 0.67 and 0.55 respectively for % predicted FEV_1 and r = 0.61 and 0.53 respectively for FEV_1/FVC). The correlations between % predicted FEV_1 and FEV_1/FVC with 15th percentile and MLD were weaker (r = 0.55 and 0.45 for % predicted FEV_1 and r = 0.49 and 0.43 for FEV_1/FVC respectively). Those results are not presented as figures.

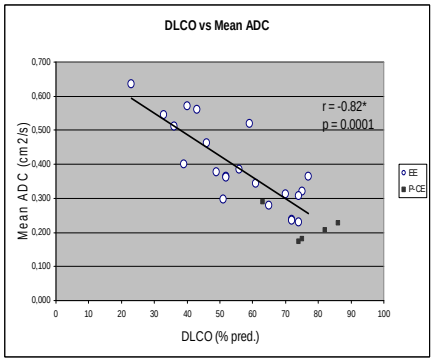

Figure 4. *Graph showing the correlation (r = -0.82) between mean ADC (apparent diffusion coefficient) from ^{3}He- MRI and percent predicted $D_{L,CO}$ (diffusing capacity of carbon monoxide) from PFT (pulmonary function test). *The correlation is significant at the 0.01 level (two-tailed). The circles represent patients with established emphysema and the squares patients with pre-clinical emphysema. The higher ADC values correspond with lower percent predicted $D_{L,CO}$ values in those patients with emphysema while lower (normal) ADC values correspond with higher (normal) % predicted $D_{L,CO}$ values in the pre-clinical group.*

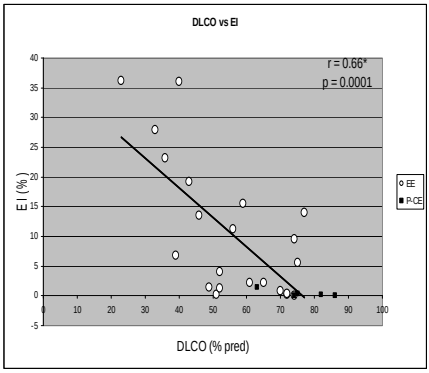

Figure 5. *Graph showing the correlation between percent predicted* $D_{L,CO}$ *(diffusing capacity of carbon monoxide) from PFT (pulmonary function test) and EI (emphysema index) from MSCT. *The correlation is significant at the 0.01 level (two-tailed).*

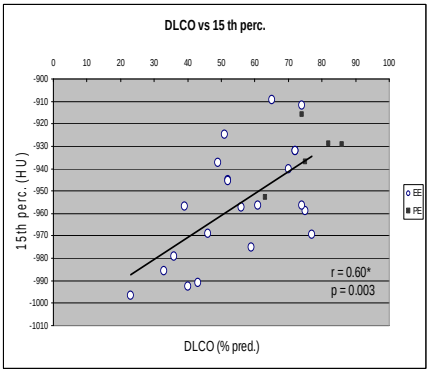

Figure 6. *Graph showing the correlation (r = 0.60) between 15th percentile point in HU from MSCT and percent predicted* $D_{L,CO}$ *(diffusing capacity of carbon monoxide) from PFT (pulmonary function test). *The correlation is significant at the 0.01 level (two-tailed). The circles represent patients with established emphysema and the squares patients with pre-clinical emphysema*

.

Paper IV

Progression of Emphysema in a 12-month Hyperpolarized ^{3}He- MRI Study: Lacunarity Analysis Provided a More Sensitive Measure than Standard ADC Analysis

Material and methods

Subjects

Thirty-nine subjects were recruited (age range 25-74 years). Twenty-two subjects had established emphysema (FEV_1 and a $D_{L,\,CO}$ < 80% of predicted values). Of the emphysema subjects, 18 had usual COPD (8 currently smoking) called COPDs, 10 ex-smoking (no smoking within the past 12 months) called COPDx, and 4 with AAT deficiency emphysema called COPDa. The 17 subjects without emphysema were 5 subjects with AAT deficiency without symptoms of emphysema, called Controla, and 12 healthy non-smoking subjects called Control.

Each subject was imaged at two lung volumes: FRC and FRC + 15% of TLC. Imaging was done at baseline, at 6 months and at 12 months for the 18 subjects with usual COPD and the healthy volunteers. The AAT-deficient subjects were imaged at baseline and at 6 months only.

Post-hoc lacunarity analysis

Lacunarity is a computationally simple texture analysis that has been used to examine growth patterns in forests (16, 17). The calculation uses a three dimensional "gliding box" of varying sizes (1x1x1 through 10x10x10 voxels). The average ADC value within the box is calculated for each position as the box moves in a voxel-by-voxel step fashion. After a collection of average values has been obtained from moving the box through the entire lung image, the mean and variance of those values are calculated. Lacunarity is then calculated as:

$$\text{Lacunarity}_i = 1 + \text{variance}^2/\text{mean}^2$$

Where "i" is the dimension of the gliding 3-dimensional box (i x i x i) and the mean and the variance are calculated as described above. To address the "edge effects" when the gliding box includes voxels outside of the lungs, the mean value for a box position was not used in the calculation of lacunarity unless ¾ of the voxels lay within the lung.

Lacunarity will tend to fall as the box size increases because of the smoothing effect of using a more course analysis results in a decrease in the variance term of the lacunarity. The value of the mean term varies very little with changes in box size. A homogenous distribution of ADC values will result in a rapid fall in lacunarity as the box size increases. The fall will be less rapid if the distribution is more

inhomogeneous. The mean ADC value for box sizes 2-6 was calculated to arrive at a single number for each image. This parameter was selected to maximize the difference between the control and the COPD lacunarity values in the reproducibility data set and was established as the lacunarity endpoint before the lacunarity of the data from this progression study was calculated.

Statistical analysis

Change and percent change from baseline were calculated for each subject. For comparisons between COPD and controls, both the healthy controls and the asymptomatic AAT subjects were used as controls. COPD-control comparisons were made using the Wilcoxon signed-rank test, which does not assume distributional properties of the changes from baseline. Changes at 6 and 12 months were tested separately. The association between endpoints was assessed using Spearman's rank correlation, which does not assume distributional properties of the endpoints. At 12 months, an additional comparison of the three groups imaged at 12 months (healthy controls, smokers with COPD and non-smokers with COPD) was performed using the Kruskal-Wallis rank test, which is a multi-group extension of the Wilcoxon signed-rank test.

Results

Figures 1-2 and Tables 1 and 2 show that during the 12–month follow-up there were no significant changes in FEV_1, $D_{L,CO}$, or mean ADC at either lung volume for any of the groups. Table 2 shows that FRC (% predicted) increased significantly ($p<0.01$ vs. baseline by paired t-test) during the first 6 months and remained elevated at 12 months for the COPDs. The change from 6 to 12 months was not statistically significant. Residual volume (RV) (% predicted) also increased during the first 6 months and remained elevated at 12 months for the COPDs but the changes were not statistically significant.

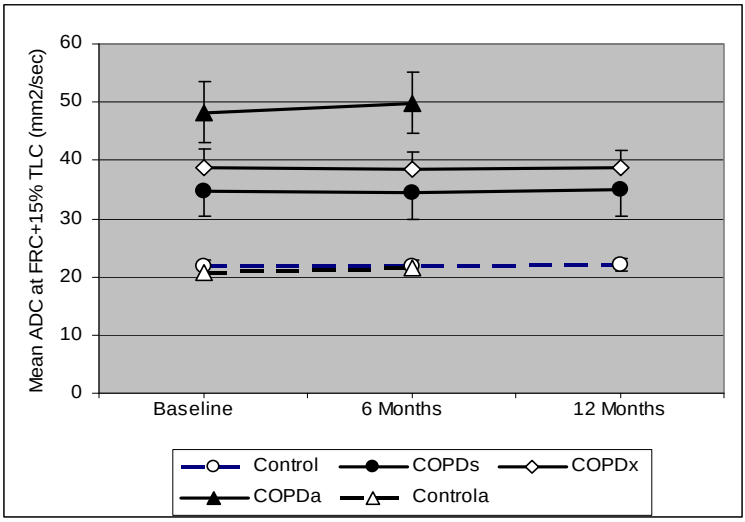

Figure 1. *Values are presented in Mean and standard error of the mean at three points of time in Controls, COPDs (smokers), COPDx (ex-smokers), COPDa (alpha-1-antitrypsin deficiency) and Controla (alpha-1-antitrypsin deficiency asymptomatic). There was no significant change in mean ADC (apparent diffusion coefficient) at 15% of TLC (total lung capacity) in the groups along the time. FRC: functional residual capacity. TLC: total lung capacity.*

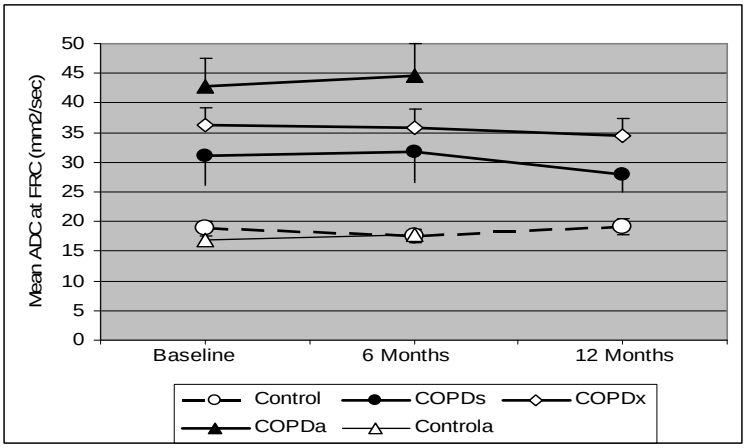

Figure 2. *Values, mean and standard error of the mean are presented in Controls, COPDs (smokers), COPDx (ex-smokers), COPDa (alpha-1-antitrypsin deficiency) and Controla (alpha-1-antitrypsin deficiency asymptomatic). There was no significant change in mean ADC (apparent diffusion coefficient) at FRC (functional residual capacity) in the groups along the time.*

***Table 1**: Lung function and lung volumes (values are mean ± s.d.)*

Subjects	FEV_1* (% predicted)			$D_{L,CO}$ * (% predicted)			FRC* (% predicted)			RV* (% predicted)		
	Base	6-mo	12-mo	Base	6-mo	12-mo	Base	6-mo	12-mo	Base	6-mo	12-mo
Control	104 ±13	103 ±15	102 ±16	95 ±10	95 ±9	93 ±8	108 ±21	113 ±23	112 ± 18	110 ±21	118 ±14	116 ±17
COPDs*	56 ±11	55 ±11	50 ±17	57 ±16	58 ±17	56 ±16	133 ±32	148 ±33	153 ± 39	173 ±44	195 ±45	204 ±59
COPDx*	47 ±10	46 ±10	46 ±10	54 ±16	56 ±17	54 ±16	129 ±26	126 ±22	127 ± 29	157 ±57	153 ±58	157 ±61
COPDa*	52 ±7	51 ±8		49 ±14	51 ±11		142 ±45	141 ±41		175 ±70	173 ±69	
Controla*	84 ±8	81 ±11		75 ±9	76 ±9		91 ±24	99 ±26		94 ±13	98 ±15	

**FEV_1: forced expiratory volume in 1 second; $D_{L,CO}$: diffusion of carbon monoxide; FRC: functional residual capacity; RV: residual volume; COPDs: COPD smokers; COPDx: COPD ex-smokers; COPDa: COPD alpha-1-antitrpsin deficiency; Controla: Control alpha-1-antitrpsin deficiency.*

Table 2: *Mean ADC (values are mean ± SD.)*

	Mean ADC (cm^2/sec)					
	FRC* + 15% TLC*			FRC		
Subjects	Base	6-mo	12-mo	Base	6-mo	12-mo
Control	0.217 ±0.040	0.217 ±0.037	0.220 ±0.038	0.188 ±0.038	0.176 ±0.037	0.191 ±0.045
COPDs*	0.348 ±0.127	0.344 ±0.131	0.350 ±0.134	0.312 ±0.140	0.318 ±0.150	0.279 ±0.083
COPDx*	0.389 ±0.097	0.384 ±0.094	0.386 ±0.100	0.363 ±0.094	0.359 ±0.095	0.346 ±0.086
COPDa*	0.483 ±0.103	0.499 ±0.106		0.428 ±0.094	0.446 ±0.108	

**FRC: forced residual capacity; TLC: total lung capacity; COPDs: COPD smokers; COPDx: COPD ex-smokers; COPDa: COPD alpha-1-antitrypsin deficiency; Controla: control alpha-1-antitrypsin deficiency*

Figure 3 and Table 3 shows the results of the post-hoc lacunarity analysis of the MR images. The mean lacunarity calculated from the ADC values acquired at FRC increased in the COPDs group at 6 months (p=0.063, NS) and at 12 months (p=0.023, significant) compared to baseline. There were no significant changes in the lacunarity at FRC in any of the other groups or in the lacunarity at FRC + 15% in any group.

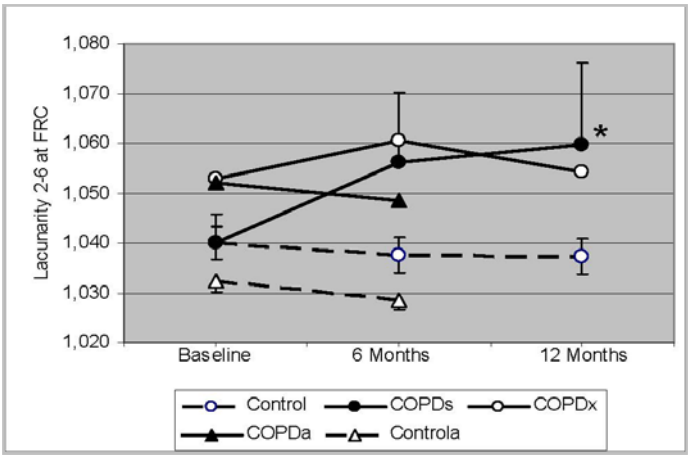

Figure 3. *Values, mean and standard error of the mean are presented in Controls, COPDs (smokers), COPDx (ex-smokers), COPDa (alpha-1-antitrypsin deficiency) and Controla (alpha-1-antitrypsin deficiency asymptomatic). Mean lacunarity increased at FRC (functional residual capacity) in the COPDs group at six and 12 months and was considered significant with $p<0.05$ vs the controls.*

Table 3*. Lacunarity (values are mean ± SD.)*

	Lacunarity					
	FRC* + 15% TLC*			FRC		
Subjects	Base	6-mo	12-mo	Base	6-mo	12-mo
Control	1.027 ± 0.007	1.024 ± 0.004	1.027 ± 0.007	1.040 ± 0.011	1.038 ± 0.012	1.037 ± 0.012
COPDs*	1.059 ± 0.053	1.062 ± 0.50	1.057 ± 0.040	1.040 ± 0.017	1.056** ± 0.040	1.060*** ± 0.046
COPDx*	1.056 ± 0.032	1.056 ± 0.030	1.055 ± 0.029	1.053 ± 0.023	1.061 ± 0.032	1.054 ± 0.028
COPDa*	1.076 ± 0.058	1.083 ± 0.075		1.103 ± 0.120	1.095 ± 0.093	
Controla*	1.022 ± 0.001	1.021 ± 0.001		1.032 ± 0.005	1.028 ± 0.004	

**FRC: forced residual capacity; TLC: total lung capacity; COPDs: COPD smokers; COPDx: COPD ex-smokers; COPDa: COPD alpha-1-antitrypsin deficiency; Controla: control alpha-1-antitrypsin deficiency. **p=0.063 (NS) vs. Control; ***p = 0.023 vs. Control.*

DISCUSSION

Paper I

Good reproducibility is fundamental in order to differentiate between normal and abnormal ADC values in the lungs. It is a prerequisite to be able to monitor the course of emphysema and to follow the results of a particular therapy.

The method of imaging the lungs and calculating the ADC has been used in animals with elastase-induced emphysema (76), in a small number of healthy adult subjects and subjects with lung disease (77-80). In these studies, the ADC values in emphysematous lungs were increased relative to ADC values obtained in subjects with healthy lungs. In another study, conducted by Salerno et al, (63) a volume of 0.35 L of helium polarised to levels from 15% to 35% and diluted to a total volume of 1.0 L with a filler with N_2 were used to investigate ADC measurements in 16 adult healthy subjects, 11 subjects with smoke-related COPD and 1 subject with alpha-1 antitrypsin deficiency (AAD) emphysema. The ADC images were homogeneous in healthy subjects, but demonstrated regional variations in diseased subjects. The ADC measurements (cm^2/sec) were significantly larger ($p<0.002$) than those for healthy subjects. Based upon the experience of the University of Virginia (63) and previous data in animals and humans, a dose of 4.5 mmol net activity and two volumes based on TLC was used to design this study in order to explore the short-term reproducibility of ADC and the appropriate volume of HP gas to use in healthy and subjects with emphysema.

The measurements of mean ADC in our study were very reproducible. The reproducibility of the mean ADC measurement within a subject is affected by the ability of the subject to lie still, to inhale the whole volume and to hold their breath during imaging. The good reproducibility in this study may in part have been due to our efforts to explain the procedure and train the subjects to cooperate to follow the protocol exactly. The results were also similar in an exploratory study (81) where the subjects did not leave the scanner between the imaging sessions. It has also been shown that different centers can achieve comparable results (82).

The clear difference in ADC values between volunteers and patients and the lack of overlap between the groups would suggest that ADC values no higher than 0.25-0.27 cm^2/sec should be expected in healthy lungs at an inhaled volume of 15% of TLC. This is in the same range as values from other studies (62, 76, 81, 83) with different diffusion gradients and volumes. However, other factors might influence the normal value, for example age.

One limitation of the present study was that the slices did not cover the

entire lung in all cases. Therefore, the overall day-to-day reproducibility could have been affected by difficulties in positioning the slices at the same location each day. One way to avoid such repositioning errors would be to use an optimized 3D sequence which could also allow for smaller voxels (83). Another limitation of diffusion ^{3}He MRI is that the ADC values on an ADC map are only derived from the lung regions in which HP ^{3}He gas reach, we obtained a measurable ADC-value although with higher SD even when only a small amount of HP ^{3}He reached an area and the signal therefore was low. This low signal however, did not appear to influence our results and the method is robust also when areas of the lung are less well ventilated.

Paper II

Once the good short-term reproducibility of ADC measurements has been shown by Morbach et al (81) in patients scanned the same day with a 20-min interval between the imaging sessions without repositioning and by (84) also in healthy volunteers and patients but scanned on three consecutive days with repositioning, the next step is to demonstrate the long-term reproducibility of the method.

Currently, the available diagnostic tools are not sensitive enough for monitoring disease progression over shorter time spans. This lack of sensitivity also prevents the evaluation of any intervention at an early stage of disease. Pulmonary function tests (PFTs) are markers of global function. Imaging tools such as computed tomography (CT) can aid in the diagnosis, but involves ionizing radiation which limits its use in longitudinal studies. Besides, CT has poor specificity for separating a fully expanded healthy lung from a lung with for example, mild emphysema (85). Hyperpolarized ^{3}He-MR imaging has emerged as a promising technique to measure structure and function in the lungs without ionizing radiation, and thereby opens up the possibility for monitoring disease progression and the effect of therapeutic efforts. The novelty of the present study is that it demonstrates good *long-term* reproducibility of ADC measurements at three different time-points (baseline, 6 months and 12 months) in a group of 12 healthy volunteers at the same centre, with the same MRI parameters and scanner. The technique seems to be sufficiently robust to have the potential to be used to investigate patients to assess the development of emphysema in COPD and in the future to evaluate the effects of drug therapies.

The correlation between mean ADC and age was not as high as that found by other groups (71, 86, 87). This may be attributed to the fact that the age distribution in our population was narrow. Nevertheless, there was a trend to higher ADC values with aging. We found that the correlation of mean ADC with age was slightly higher in the apical regions of the lung, supporting

the theory that aging causes changes resembling emphysema in COPD with the same distribution pattern as COPD-related emphysema (88-90). Age affects the interpretation of results and should therefore be taken into account when normative data are established.

We found a significant difference in mean ADC between the most anterior compared to the most posterior regions of the lung. This is in accordance with results presented by other groups for healthy subjects (63, 79, 83, 91-93). This difference has been explained by the gravitational compression of the alveoli in the most posterior regions of the lung when in the supine position. This assumption is supported by the examination of one volunteer (data is not included in the analysis in this study) in both supine and prone position in which mean ADC was higher in the highest slices in both positions, although the difference was smaller in the prone position. We did not find significant apical-basal regional differences in mean ADC in the lungs. We attribute this to the fact that we measured the ADC of the ROI in the most peripheral regions to avoid bias from the high ADC values from the bronchial segments and the fact that the subjects were in the supine position.

Limitations of the present study are: the small sample size which diminishes the power of the study; the selection of the patients, which was not age-matched and could explain the relative low correlation when compared to other groups. Besides, it is very difficult to now how much of the ADC value which should be attributed to disease and how much to aging because there is no established normal range for mean ADC values. Looking at what has been proposed as 'normal' in healthy human lungs shows that the variation is high between research groups. The lowest mean ADC value described has been 0.17 cm^2/s by Morbach et al.(81) and the highest 0.24 cm^2/s by Altes et al. (86). This can be explained by the different techniques used by different groups. Our mean ADC value is 0.21 cm^2/s but one subject had a mean ADC at 0.29 cm^2/s which is in the range of values found in early-stage emphysema patients. The subjects had all been included based on the same inclusion criteria using spirometric parameters of normality. This indicates that results from spirometry may overlap between normal and abnormal patients.

Paper III

The present study compares the mean ADC from HP ^{3}He MRI with data from MSCT and PFT, especially % predicted $D_{L,CO}$, for the diagnosis of emphysema. It is one of the first studies that compare data from different techniques. Our data demonstrate good-to-excellent agreement between mean ADC from MRI and quantitative data from MSCT and PFT, whereas MSCT data correlated less well with PFT especially % predicted $D_{L,CO}$.

Although lung densitometry for the assessment of pulmonary emphysema

with CT has been compared to pathology (94), pulmonary function and health status, there is not yet any method regarded as a fully optimized and standardized evaluation technique for CT images. The results of the National Emphysema Treatment Trial study by Naunheim et al (95) and more recently Madani et al (33) suggest that imaging of the whole lungs with MSCT is a more appropriate technique. We therefore used whole lung MSCT for the comparison with MRI data.

Mean lung density (MLD) and 15th percentile point did not show a large decrease in our emphysema patients compared to the pre-clinical emphysema group contrary to expectations. The EI was however increased. MLD calculated by averaging the densities of all pixels in the image that represents the lungs has been found to be less reproducible and therefore less sensitive to density changes than other densitometry parameters (96). The percentile point has been compared to PFT (22) and pathology (23). As described by Stoel (25) and Stolk (97), the RA and the nth percentile point are closely related, since they are each other's inverse function. However, RA has less discrimination power and its sensitivity is highly dependent on the threshold used, while in the nth percentile point, each percentile corresponds to a distinct density value and its sensitivity is therefore less dependent of the choice of percentile. This advantage made us choose the 15th percentile as one of the reference measurements of emphysema by MSCT. Standardization of the optimal Emphysema Index (EI) threshold remains unsolved. We decided to use the threshold -950 HU based on the results of the study by Genevois (98), which showed the threshold -950 HU to be the one best correlating with emphysema. However, consideration must be taken to the study by Dirksen et al (24) which suggests the percentile point to be more robust than the emphysema index.

Our results showed stronger correlation between mean ADC and % predicted $D_{L,CO}$ ($r = 0.82$) than between EI and % predicted $D_{L,CO}$ ($r = 0.66$) as well as between 15th percentile and % predicted $D_{L,CO}$ ($r = 0.60$) and MLD and % predicted $D_{L,CO}$ ($r = 0.29$). The difference seems to be that some patients with a low EI still have a high mean ADC.

One limitation in our study was the difference in the inspired volumes at the examinations. The MRI images were generated at FRC + 15% of TLC and the MSCT images at TLC. Consequently, differences in alveolar volume may influence our results. However, it has been shown that the value of the ADC depends on the inhaled volume with a higher ADC if a larger volume is inhaled (84). This suggests that the mean ADC would have been higher at TLC and the sensitivity for small changes even higher if MRI had been performed at TLC. This would have further enhanced the difference from MSCT indices

shown. Further, air trapping could represent a limitation in our study, since the gas reaches areas that are well ventilated. We tried to avoid this by the use of an individually adjusted volume of gas. The inhaled volume of ^{3}He was adjusted to 15% of the TLC of each patient in order to assure that the gas was distributed throughout the lungs. It has also been shown earlier (84) that this dose seems to be enough to avoid serious air trapping. Besides, special emphasis was made in training all patients to breathe appropriately.

The current study confirms that mean ADC clearly depicts emphysema-related changes, correlates well with emphysema index and other parameters from CT. It also seems to correlate better with % predicted $D_{L,CO}$ than parameters derived from CT measurements and does this without using ionizing radiation.

Paper IV

The study showed unequivocally that mean ADC did not detect disease progression of mild emphysema in COPD patients within 6-12 months. However, the study provided considerable information about techniques that may be able to detect progression in a subset of COPD patients. As expected, FEV_1 and $D_{L,CO}$ also failed to detect progression in any of the COPD groups. However, every COPDs subject showed an increase in FRC at 6 months resulting in a statistically significant increase for this group. This change of FRC was surprising and may be related to the progression of air trapping in the lungs in this population. Air trapping would be expected also to increase the mean RV, which did occur in this group, but the changes were not statistically significant.

Mean ADC is the most commonly used biomarker of lung structure obtained from MR imaging of the lungs with hyperpolarized gas. But, it has an inherent limitation because it ignores the spatial information that is contained in the ADC images. We analyzed the data with a more global texture analysis, lacunarity, which would quantify the inhomogeneities of the distribution of ADC values that should increase as emphysema progresses (99). The lacunarity of the ADC maps increased significantly at 12 months but only for the images obtained at FRC and only for the COPDs group. Many questions arose from this surprising result and we tried to analyze each factor that could be relevant to explain it. The first consideration we made was that emphysema is a slowly progressing disease. Therefore the changes that occur within 12 months are usually very small. Firstly, imaging the lungs at FRC may have amplified the structural changes because air trapping would tend to increase the size of the large alveoli and decrease the size of the smaller normal alveoli and thereby increase the inhomogeneities that lacunarity is measuring. Secondly, the lack of lacunarity increase in COPDa

can be explained by the inherent differences in the pathology between these two types of COPD. Emphysema due to smoking occurs primarily in the upper lobes and it is more "patchy" than emphysema due to AAT deficiency which occurs primarily in the lower lobes. In the latter, the destruction of the alveolar walls is more evenly distributed and results in a more homogeneous size distribution of the enlarged alveoli (100). Thirdly, the lack of lacunarity increase in the COPDx group might be explained by the variability of response that may well reflect the true variability in the biological effects that occur after smoking cessation. Fourthly, lacunarity increased more in the first 6 month and this might be attributed to seasonal differences because the first 6 months were from June to December for all subjects. However, there were no obvious differences in the number of exacerbations or other adverse events reported in the two periods. Fifthly, at first sight, the most surprising finding was that lacunarity was the same for the COPDs and control subjects at baseline. One of the reasons for the similarity of the lacunarites at baseline is that two of the 8 COPDs subjects may have had no emphysema at all. Removing the two subjects separates the baseline values and also increases the relative size of the changes with time in the other 6 subjects. Another reason for the similarity of the lacunarity values at baseline lies in the formula for lacunarity. As emphysema progresses, both the variance and the mean would increase. Therefore, in the earlier stages of emphysema development, the mean and the variance may increase to a similar degree, which would tend to minimize changes in lacunarity.

In subjects who have established emphysema and who are currently smoking, the use of all of the spatial information collected from the ADC maps for textural analysis might provide a biomarker of disease progression. However, further studies are necessary to validate these results in a prospective study with a larger group of subjects.

GENERAL SUMMARY AND DISCUSSION

Functional imaging of the lung has developed from nuclear medicine techniques in the past to MSCT and MRI with intravenous or inhaled contrast media nowadays. Both modalities have developed fast and provide the radiologist with detailed and regional information about respiratory mechanics, ventilation, gas exchange and perfusion. MRI has, in fact, contributed most to functional imaging of the lung in the recent years. Among lung parenchyma diseases emphysema has been in focus particularly with inhaled gases HP *i.e.* ^{3}He. Several factors must be considered regarding the HP technique such as dose delivery, MR scanner, sequences, data analysis, costs, etc.

Each hyperpolarisation technique has advantages and disadvantages that are based mainly in economical aspects. Spin-exchange technique is relatively easier to perform than metastability exchange technique and reaches approximately 30-40% polarisation without enrichment techniques, but it is only for the moment capable of producing 1 L of HP ^{3}He per 24 hours. This amount allows performing four to six MR sequences per day. The metastability exchange technique used today can produce up to 25 L of gas reaching polarisation levels up to 50-80% in 24 hours. This opens for the possibility of a centralized production with a distribution network if the appropriate infrastructure is available. In this way the costs could diminish. Optimization of the best technique to hyperpolarize the gas is important due to the limited accessibility to helium in nature. This restriction contributes to increased costs. One possibility to overcome this difficulty is to bring helium from the moon. This is not an inconceivable option as there already is the possibility to 'travelling' outside the earth as a tourist attraction. Actually, as ^{3}He also is an important part of the fusion technique for energy production there is an increasing interest in lunar ^{3}He. As an example, on October 22th 2008 India sent up a satellite with the outspoken purpose of exploring the amounts of ^{3}He around the moon.

HP ^{3}He can be delivered to the subject by two different methods. One way is through a tube connected to a plastic bag. This method uses a mixture of ^{3}He in N_2, giving an anoxic breath. This method has the advantages of being easy to perform, fast and clean. It is also easy to control the volume of gas mixture to be inhaled. However, disadvantages are that an anoxic breath can be difficult for very impaired patients that are in lying supine in the scanner. It is also not possible to recycle the ^{3}He-gas easily. Alternatively, the gas can be administered by a mouthpiece using a delivery device. The dose is administered as a bolus of approximately 50-500 ml. One advantage of this method is that the dose of gas can be administered at an

arbitrarily set point during inspiration. Additionally, the applicator device allows recovery of the exhaled ^{3}He, allowing recycling and consequently reducing costs. One disadvantage is that the inhaled volume of gas mixture is decided by the patient which could reduce the reproducibility. Another disadvantage is that the oxygen content in the mixture of ^{3}He and air depolarises the ^{3}He to a certain extent which reduces the signal. We decided to use the bag system because we wanted to control the volume of gas administered to the patient and both to establish any volume dependency and to obtain a high level of reproducibility.

The MR scanners most widely used for HP ^{3}He are 1.5 T systems because this is the standard field strength in clinical practice. However, MR scanners are expensive and require an expert team to get the best results. Moreover, MR scanners are less available at radiology departments all over the world than CT. The technical requirements for MRI with HP ^{3}He are even more specific: the MR system requires broadband or multiband capability and special RF coils. These factors all increase the costs.

There are three major aspects that must be taken into account when an imaging strategy for HP gas is chosen. Firstly, the non-recoverable hyperpolarisation of the spin population puts restrictions on the pulse sequences employed. Secondly, the introduction of oxygen from the airways leads to loss of polarization through T1 relaxation. Thirdly, the high diffusion coefficient of ^{3}He at atmospheric pressure (D≈1.8 x 10^{-4}cm^{2}s^{-1}) results in measurable signal loss even for the gradient waveforms used for routine imaging. Therefore, fast imaging sequences must be used such as FLASH, FISP, RARE and EPI. We used a FLASH sequence because at the moment we started our studies it was the most used method for this kind of research. In this way our results could be comparable with other research groups.

To provide more information of lung microstructure it has recently been proposed (68) to use a range of time scales. This technique could provide information of different parts i.e. using a very short timescale would provide information about the alveoli while a long timescale would provide information about the bronchioles. Another way to obtain more detailed information of lung microstructure may be the use of 3D imaging sequences with high spatial resolution.

COPD is an increasing health problem being one of the most prevalent causes of morbidity and mortality worldwide. It is currently a global health priority (5). It is of extreme importance not only to make an accurate diagnosis in those patients who already have a deteriorated lung function and in those who are symptomatic but also in those patients who have an early or mild disease and are asymptomatic. MRI is of particular interest for the functional in vivo evaluation of patients with COPD. It

can provide both functional and morphological information with the advantage of not using ionizing radiation. Despite large advances in this field in the last years, there is a need for validation of one method to establish a standard protocol that can be used. Thereby, the results can be comparable between different centres. This standardized protocol must include: sequence, b-values, flip angle, diffusion gradient direction, etc., as well as the ^{3}He application technique and data analysis. Only this way normal reference values can be established. Further validation using the morphological and functional standards of reference also has to be made. If this is achieved, MRI could become a useful imaging modality in the assessment of early emphysema and in the follow-up of patients under medical therapy.

CONCLUSIONS AND FINAL REMARKS

The general aim of this work was to evaluate the potential of hyperpolarized ^{3}He-diffusion MRI technique to diagnose early emphysema changes in the lungs.

This work supports the following conclusions:

✓ ADC measurement with HP ^{3}He MR imaging was highly reproducible, sensitive to small differences in alveolar size, and clearly separates volunteers and patients with mild to moderate emphysema. Dependency on inhaled volume of gas was shown, and the higher volume, 15% of TLC, seemed preferable.

✓ The long-term reproducibility of the ADC in healthy volunteers was good. There was a correlation between mean ADC and age, which means that age must be taken into account when judging the absence or presence of emphysematous disease changes based on ^{3}He MR imaging.

✓ Mean ADC clearly depicted emphysema-related changes, correlated well with emphysema index and the 15th percentile. The correlation between $D_{L,CO}$ and ^{3}He MRI was better than with CT.

✓ The mean ADC calculated from the data obtained by ^{3}He MR imaging was not able to detect emphysema progression within 12 months in this study. However, it all the spatial information collected from the ADC maps was used for a textural analysis, in this case, lacunarity analysis it could provide a biomarker of disease progression in subjects who had established emphysema and who were currently smoking.

In addition to these conclusions, the combination of MR imaging, hyperpolarized gases, and the proper textural analysis of the data could provide a powerful investigative tool for understanding the pathophysiology of emphysema and evaluation of therapies designed to alter the course of disease even if economic obstacles prohibit a widespread use.

ACKNOWLEDGMENTS

I wish to express my sincere gratitude to all those people who in different ways assisted me in this work. Especially I want to thank:

Olle Ekberg, Professor, for his encouragement, enthusiasm, and support throughout the study and providing me excellent working conditions;

Per Åkeson, Associated Professor, the principal investigator of this project, for his scientific training and guidance, his never ending amount of new ideas and for introducing me in the exciting research world and most of all for his patience to correct all my written failures;

Peter Leander, Associated Professor, the Head of our institution, for his interest, support and for giving me time to think and write this thesis;

Per Wollmer, Professor, for his invaluable support in lung physiology and his continuous encouragement;

Eeva Piitulainen, Associated Professor, Respiratory department, for providing all the subjects examined in this study and her knowledge in lung pathology;

Ingrid Casselbrant, MD, Respiratory department, for her excellent clinical knowledge, patient management and control of all the factors during the clinical trials and everlasting enthusiasm and exactitude;

Peter Magnusson, PhD, for his hard work with the physics and measurements, and his effectiveness in this study;

Harvey Fountaine, project leader at Amersham Healthcare now GE Health Care, for his invaluable support;

Göran Pettersson, PhD, Healthcare now GE Health Care, for his effectiveness and for doing a lot of the practical work;

Barry Peterson, PhD, Pfizer USA, for his tenacity, enthusiasm, support and punctual reviewing of drafts throughout the study;

Curt Johansson, MSc, Radiology department, for his assistance in conducting the MR imaging and his everlasting humour and attitude;

Isabella Björk, MSc, Respiratory department, for her assistance in the clinical trials especially with the breathing training;

Georg Hanson, MSc, Healthcare now GE Health Care, for daily running up and down with the ^{3}He bag and give it to the patients;

Birgit Persson, Healthcare now GE Health Care, for her assistance in the hyperpolarization process;

Klaes Golman, Professor, Amersham Healthcare now GE Health Care, for creating a special research environment and for his support;

Birgitta Hillarp, Associated Professor, Radiology department, and Head of the thoracic section, clinical tutor, for giving me the opportunity to participate in this research project and her encouragement throughout the study;

Jan Wolber and **Paul Gordon**, PhDs, Amersham Healthcare now GE Health Care, for their sharp-eyed and helpful criticism;

Eufrozina Selariu, MD, radiology department, for friendship, encouragement and never ending support;

Barbara Elmståhl and **Sophia Zackrisson** PhD, MD, colleagues and friends, for their encouragement, enthusiasm and help in the last step of this work;

Eva Prahl, Radiology department, for her enormous work with typewriting, correcting and editing this thesis and always willing to help;

And finally my family, **Juan and Gabriel**, for enormous patience and never ending support, without whom this thesis would not have been possible.

This study was sponsored by Amersham Healthcare, now GE Health Care, Little Chalfont, UK and Pfizer Inc., Groton, CT, USA.

REFERENCES

1. GOLD. Global strategy for the diagnosis, management, and prevention of chronic obstructive lung disease; 2007 (update).
2. WHO. World health report. Geneve; 2000.
3. Lopez AD, Shibuya K, Rao C, Mathers CD, Hansell AL, Held LS, Schmid V, Buist S. Chronic obstructive pulmonary disease: Current burden and future projections. *Eur Respir J* 2006;27:397-412.
4. Murray CJ, Lopez AD. Alternative projections of mortality and disability by cause 1990-2020: Global burden of disease study. *Lancet* 1997;349:1498-1504.
5. Rabe KF, Hurd S, Anzueto A, Barnes PJ, Buist SA, Calverley P, Fukuchi Y, Jenkins C, Rodriguez-Roisin R, van Weel C, et al. Global strategy for the diagnosis, management, and prevention of chronic obstructive pulmonary disease: Gold executive summary. *Am J Respir Crit Care Med* 2007;176:532-555.
6. Standards for the diagnosis and care of patients with chronic obstructive pulmonary disease (copd) and asthma. This official statement of the American Thoracic Society was adopted by the ATS Board of Directors, November 1986. *Am Rev Respir Dis* 1987;136:225-244.
7. The definition of emphysema. Report of a national heart, lung, and blood institute, division of lung diseases workshop. *Am Rev Respir Dis* 1985;132:182-185.
8. Pratt PC. Emphysema and chronic airways disease. New York: Springer-Verlag; 1994.
9. Snider GL. Distinguishing among asthma, chronic bronchitis, and emphysema. *Chest* 1985;87:35S-39S.
10. Heitzman ER, Markarian B, Berger I, Dailey E. The secondary pulmonary lobule: A practical concept for interpretation of chest radiographs. I. Roentgen anatomy of the normal secondary pulmonary lobule. *Radiology* 1969;93:507-512.
11. Heitzman ER, Markarian B, Berger I, Dailey E. The secondary pulmonary lobule: A practical concept for interpretation of chest radiographs. Ii. Application of the anatomic concept to an understanding of roentgen pattern in disease states. *Radiology* 1969;93:513-519.
12. Reid L. The secondary lobule in the adult human lung, with special reference to its appearance in bronchograms. *Thorax* 1958;13:110-115.
13. Fraser RG PJ, Paré PD, Fraser RS, Genereux GP. Disease of the airways. Philadelphia: Saunders; 1990.

14. Spencer H. Pathology of the lung. Emphysema. Philadelphia: Saunders; 1977.
15. Thurlbeck WM. Chronic air flow obstruction. New York: Thieme; 1988.
16. Cockcroft DW, Horne SL. Localization of emphysema within the lung. An hypothesis based upon ventilation/perfusion relationships. *Chest* 1982;82:483-487.
17. Guenter CA, Welch MH, Hammarsten JF. Alpha 1 antitrypsin deficiency and pulmonary emphysema. *Annu Rev Med* 1971;22:283-292.
18. Welch MH, Reinecke ME, Hammarsten JF, Guenter CA. Antitrypsin deficiency in pulmonary disease: The significance of intermediate levels. *Ann Intern Med* 1969;71:533-542.
19. Goddard PR, Nicholson EM, Laszlo G, Watt I. Computed tomography in pulmonary emphysema. *Clin Radiol* 1982;33:379-387.
20. Rosenblum LJ, Mauceri RA, Wellenstein DE, Bassano DA, Cohen WN, Heitzman ER. Computed tomography of the lung. *Radiology* 1978;129:521-524.
21. Muller NL, Staples CA, Miller RR, Abboud RT. "Density mask". An objective method to quantitate emphysema using computed tomography. *Chest* 1988;94:782-787.
22. Gould GA, Redpath AT, Ryan M, Warren PM, Best JJ, Flenley DC, MacNee W. Lung CT density correlates with measurements of airflow limitation and the diffusing capacity. *Eur Respir J* 1991;4:141-146.
23. Gould GA, MacNee W, McLean A, Warren PM, Redpath A, Best JJ, Lamb D, Flenley DC. CT measurements of lung density in life can quantitate distal airspace enlargement - an essential defining feature of human emphysema. *Am Rev Respir Dis* 1988;137:380-392.
24. Dirksen A, Friis M, Olesen KP, Skovgaard LT, Sörensen K. Progress of emphysema in severe alpha-1-antitrypsin deficiency as assessed by annual CT. *Acta Radiol* 1997;38:826-832.
25. Stoel BC, Stolk J. Optimization and standardization of lung densitometry in the assessment of pulmonary emphysema. *Invest Radiol* 2004;39:681-688.
26. Uppaluri R, Hoffman EA, Sonka M, Hartley PG, Hunninghake GW, McLennan G. Computer recognition of regional lung disease patterns. *Am J Respir Crit Care Med* 1999;160:648-654.
27. Uppaluri R, Mitsa T, Sonka M, Hoffman EA, McLennan G. Quantification of pulmonary emphysema from lung computed

tomography images. *Am J Respir Crit Care Med* 1997;156:248-254.

28. Rationale and design of the national emphysema treatment trial (nett): A prospective randomized trial of lung volume reduction surgery. *J Thorac Cardiovasc Surg* 1999;118:518-528.
29. Fishman A, Martinez F, Naunheim K, Piantadosi S, Wise R, Ries A, Weinmann G, Wood DE. A randomized trial comparing lung-volume-reduction surgery with medical therapy for severe emphysema. *N Engl J Med* 2003;348:2059-2073.
30. Hoffman EA, Simon BA, McLennan G. State of the art. A structural and functional assessment of the lung via multidetector-row computed tomography: Phenotyping chronic obstructive pulmonary disease. *Proc Am Thorac Soc* 2006;3:519-532.
31. Mishima M, Hirai T, Itoh H, Nakano Y, Sakai H, Muro S, Nishimura K, Oku Y, Chin K, Ohi M, et al. Complexity of terminal airspace geometry assessed by lung computed tomography in normal subjects and patients with chronic obstructive pulmonary disease. *Proc Natl Acad Sci U S A* 1999;96:8829-8834.
32. Studler U, Gluecker T, Bongartz G, Roth J, Steinbrich W. Image quality from high-resolution ct of the lung: Comparison of axial scans and of sections reconstructed from volumetric data acquired using MDCT. *AJR Am J Roentgenol* 2005;185:602-607.
33. Madani A, De Maertelaer V, Zanen J, Gevenois PA. Pulmonary emphysema: Radiation dose and section thickness at multidetector CT quantification--comparison with macroscopic and microscopic morphometry. *Radiology* 2007;243:250-257.
34. Brown MA, Semelka RC. MR imaging abbreviations, definitions, and descriptions: A review. *Radiology* 1999;213:647-662.
35. Westbrook C KC. MRI in practice. Oxford, England: Blackwell Science; 1998.
36. Hahn E. Spin echoes. *Phys Rev* 1950;80:580-594.
37. Twieg DB. The k-trajectory formulation of the NMR imaging process with applications in analysis and synthesis of imaging methods. *Med Phys* 1983;10:610-621.
38. Mansfield P. Multiplanar image formation using NMR spin echoes. *J Phys C Solid State Phys* 1977;10:L55-L-58.
39. Stejskal E. Spin diffusion measurements: Spin-echoes in the presence of a time-dependent field gradient. *J Chem Phys* 1965;42:288-292.

40. Herold C, Zerhouni, EA. The mediastinum and lungs. In: Higgins CB HH, Helms CA, editor. Magnetic resonance imaging of the body. New York: Raven Press; 1992. p. 461-523.
41. Kauczor H, Surkau R, Roberts T. MRI using hyperpolarized noble gases. *Eur Radiol* 1998;8:820-827.
42. Wittenberg L, Santarius, JF, Kulcinski GL. Lunar source of ^{3}he for commercial fusion power. *Fusion Technol* 1986;10:167-178.
43. Aziz TS. Xenon in anesthesia. *Int Anesthesiol Clin* 2001;39:1-14.
44. Burov NE, Dzhabarov DA, Ostapchenko DA, Kornienko L, Shulunov MV. [clinical stages and subjective sensations in xenon anesthesia]. *Anesteziol Reanimatol* 1993:7-11.
45. Saam B, Happer W, Middleton H. Nuclear relaxation of 3he in the presence of o2. *Phys Rev A* 1995;52:862-865.
46. Albert MS, Cates GD, Driehuys B, Happer W, Saam B, Springer CS, Jr., Wishnia A. Biological magnetic resonance imaging using laser-polarized 129xe. *Nature* 1994;370:199-201.
47. Mugler JP, 3rd, Driehuys B, Brookeman JR, Cates GD, Berr SS, Bryant RG, Daniel TM, de Lange EE, Downs JH, 3rd, Erickson CJ, et al. MR imaging and spectroscopy using hyperpolarized 129xe gas: Preliminary human results. *Magn Reson Med* 1997;37:809-815.
48. Bachert P, Schad LR, Bock M, Knopp MV, Ebert M, Grossmann T, Heil W, Hofmann D, Surkau R, Otten EW. Nuclear magnetic resonance imaging of airways in humans with use of hyperpolarized 3he. *Magn Reson Med* 1996;36:192-196.
49. Ebert M, Grossmann T, Heil W, Otten WE, Surkau R, Leduc M, Bachert P, Knopp MV, Schad LR, Thelen M. Nuclear magnetic resonance imaging with hyperpolarised helium-3. *Lancet* 1996;347:1297-1299.
50. MacFall JR, Charles HC, Black RD, Middleton H, Swartz JC, Saam B, Driehuys B, Erickson C, Happer W, Cates GD, et al. Human lung air spaces: Potential for MR imaging with hyperpolarized he-3. *Radiology* 1996;200:553-558.
51. Panth SRF, S. Holmes, J. Fuller, S. Korosec, F. Grist, T. Assessment of lung ventilation, gas trapping and pulmonary perfusion in patients with asthma during inhaled corticosteroid withdrawal. Proceedings of the 12th Annual Meeting of ISMRM. Kyoto, Japan; 2004.
52. Tzeng YM, J. Shah, N. et al. Quantification of ventilation heterogeneity from hyperpolarized ^{3}he MR images using coefficient of variation. In: Proceedings of the 13th Annual

Meeting of the ISMRM. Miami Beach, FL. USA; 2005.

53. Gast KK, Zaporozhan J, Ley S, Biedermann A, Knitz F, Eberle B, Schmiedeskamp J, Heussel CP, Mayer E, Schreiber WG, et al. (3)he-MRI in follow-up of lung transplant recipients. *Eur Radiol* 2004;14:78-85.
54. Zaporozhan J, Ley S, Gast KK, Schmiedeskamp J, Biedermann A, Eberle B, Kauczor HU. Functional analysis in single-lung transplant recipients: A comparative study of high-resolution CT, 3he-MRI, and pulmonary function tests. *Chest* 2004;125:173-181.
55. Dupuich D, Berthezene Y, Clouet PL, Stupar V, Canet E, Cremillieux Y. Dynamic 3he imaging for quantification of regional lung ventilation parameters. *Magn Reson Med* 2003;50:777-783.
56. Gast KK, Puderbach MU, Rodriguez I, Eberle B, Markstaller K, Hanke AT, Schmiedeskamp J, Weiler N, Lill J, Schreiber WG, et al. Dynamic ventilation (3)he-magnetic resonance imaging with lung motion correction: Gas flow distribution analysis. *Invest Radiol* 2002;37:126-134.
57. McMahon CJ, Dodd JD, Hill C, Woodhouse N, Wild JM, Fichele S, Gallagher CG, Skehan SJ, van Beek EJ, Masterson JB. Hyperpolarized 3helium magnetic resonance ventilation imaging of the lung in cystic fibrosis: Comparison with high resolution CT and spirometry. *Eur Radiol* 2006;16:2483-2490.
58. Eberle B, Weiler N, Markstaller K, Kauczor H, Deninger A, Ebert M, Grossmann T, Heil W, Lauer LO, Roberts TP, et al. Analysis of intrapulmonary o(2) concentration by MR imaging of inhaled hyperpolarized helium-3. *J Appl Physiol* 1999;87:2043-2052.
59. Jalali A, Ishii M, Edvinsson JM, Guan L, Itkin M, Lipson DA, Baumgardner JE, Rizi RR. Detection of simulated pulmonary embolism in a porcine model using hyperpolarized 3he MRI. *Magn Reson Med* 2004;51:291-298.
60. Chen XJ, Moller HE, Chawla MS, Cofer GP, Driehuys B, Hedlund LW, Johnson GA. Spatially resolved measurements of hyperpolarized gas properties in the lung in vivo. Part i: Diffusion coefficient. *Magn Reson Med* 1999;42:721-728.
61. Chen XJ, Moller HE, Chawla MS, Cofer GP, Driehuys B, Hedlund LW, MacFall JR, Johnson GA. Spatially resolved measurements of hyperpolarized gas properties in the lung in vivo. Part ii: T *(2). *Magn Reson Med* 1999;42:729-737.
62. Saam BT, Yablonskiy DA, Kodibagkar VD, Leawoods JC,

Gierada DS, Cooper JD, Lefrak SS, Conradi MS. MR imaging of diffusion of (3)he gas in healthy and diseased lungs. *Magn Reson Med* 2000;44:174-179.

63. Salerno M, de Lange EE, Altes TA, Truwit JD, Brookeman JR, Mugler JP, 3rd. Emphysema: Hyperpolarized helium 3 diffusion MR imaging of the lungs compared with spirometric indexes--initial experience. *Radiology* 2002;222:252-260.
64. Durand E, Guillot G, Darrasse L, Tastevin G, Nacher PJ, Vignaud A, Vattolo D, Bittoun J. CPMG measurements and ultrafast imaging in human lungs with hyperpolarized helium-3 at low field (0.1 t). *Magn Reson Med* 2002;47:75-81.
65. Owers-Bradley JR, Fichele S, Bennattayalah A, McGloin CJ, Bowtell RW, Morgan PS, Moody AR. MR tagging of human lungs using hyperpolarized 3he gas. *J Magn Reson Imaging* 2003;17:142-146.
66. Yablonskiy DA, Sukstanskii AL, Leawoods JC, Gierada DS, Bretthorst GL, Lefrak SS, Cooper JD, Conradi MS. Quantitative in vivo assessment of lung microstructure at the alveolar level with hyperpolarized 3he diffusion MRI. *Proc Natl Acad Sci U S A* 2002;99:3111-3116.
67. Woods JC, Yablonskiy DA, Choong CK, Chino K, Pierce JA, Hogg JC, Bentley J, Cooper JD, Conradi MS, Macklem PT. Long-range diffusion of hyperpolarized 3he in explanted normal and emphysematous human lungs via magnetization tagging. *J Appl Physiol* 2005;99:1992-1997.
68. Mugler JP, 3rd, Wang C, Miller GW, Cates GD, Jr., Mata JF, Brookeman JR, de Lange EE, Altes TA. Helium-3 diffusion MR imaging of the human lung over multiple time scales. *Acad Radiol* 2008;15:693-701.
69. Kober F, Koenigsberg B, Belle V, Viallon M, Leviel JL, Delon A, Ziegler A, Decorps M. NMR imaging of thermally polarized helium-3 gas. *J Magn Reson* 1999;138:308-312.
70. Shanbhag DD, Altes TA, Miller GW, Mata JF, Knight-Scott J. Q-space analysis of lung morphometry in vivo with hyperpolarized 3he spectroscopy. *J Magn Reson Imaging* 2006;24:84-94.
71. Fain SB, Altes TA, Panth SR, Evans MD, Waters B, Mugler JP, 3rd, Korosec FR, Grist TM, Silverman M, Salerno M, et al. Detection of age-dependent changes in healthy adult lungs with diffusion-weighted 3he MRI. *Acad Radiol* 2005;12:1385-1393.
72. Happer W ME, Schaefer S, Schreiber D, Wijngaarden W, Zeng X. Polarization of the

nuclear spins of noble-gas atoms by spin-exchange with optically pumped alkali-metal atoms. *Phys Rev A* 1984;29:3092-3110.

73. Edelstein WA, Bottomley PA, Pfeifer LM. A signal-to-noise calibration procedure for NMR imaging systems. *Med Phys* 1984;11:180-185.
74. Henkelman RM. Measurement of signal intensities in the presence of noise in MR images. *Med Phys* 1985;12:232-233.
75. Siafakas NM, Vermeire P, Pride NB, Paoletti P, Gibson J, Howard P, Yernault JC, Decramer M, Higenbottam T, Postma DS, et al. Optimal assessment and management of chronic obstructive pulmonary disease (copd). The European respiratory society task force. *Eur Respir J* 1995;8:1398-1420.
76. Chen XJ, Hedlund LW, Moller HE, Chawla MS, Maronpot RR, Johnson GA. Detection of emphysema in rat lungs by using magnetic resonance measurements of 3he diffusion. *Proc Natl Acad Sci U S A* 2000;97:11478-11481.
77. Mugler III JP, Brookeman JR, Knight-Scott J. Regional measurement of the ^{3}he diffusion coefficient in the human lung. Proc Intl Soc Mag Reson Med, 6th Meeting. Sydney, Australia; 1998.
78. Saam B, Yablonskiy DA, Gierada DS, Conradi MS. Rapid imaging of hyperpolarized gas using epi. *Magn Reson Med* 1999;42:507-514.
79. Salerno MB, J. de Lange, EE. Knight-Scott, J. Mugler III, JP. Demonstration of an alveolar-size gradient in the healthy human lung: A study of reproducibility of hyperpolarized ^{3}he diffusion MRI. In: Proc of ISMRM 8th Annual Meeting, Denver, CO, USA. 2000.
80. Salerno MB, J. de Lange, EE. Knight-Scott, J. Mugler III, JP. Detection of regional microstructural changes of the lung in emphysema using hyperpolarized ^{3}he diffusion MRI. Proc Intl Soc Magn Reson Med, 8th Meeting. Denver, Colorado, USA; 2000.
81. Morbach AE, Gast KK, Schmiedeskamp J, Dahmen A, Herweling A, Heussel CP, Kauczor HU, Schreiber WG. Diffusion-weighted mri of the lung with hyperpolarized helium-3: A study of reproducibility. *J Magn Reson Imaging* 2005;21:765-774.
82. Schreiber WG, Morbach AE, Stavngaard T, Gast KK, Herweling A, Sogaard LV, Windirsch M, Schmiedeskamp J, Heussel CP, Kauczor HU. Assessment of lung microstructure with magnetic resonance imaging of hyperpolarized helium-3. *Respir*

Physiol Neurobiol 2005;148:23-42.

83. Swift AJ, Wild JM, Fichele S, Woodhouse N, Fleming S, Waterhouse J, Lawson RA, Paley MN, Van Beek EJ. Emphysematous changes and normal variation in smokers and copd patients using diffusion 3he MRI. *Eur J Radiol* 2005;54:352-358.
84. Diaz S, Casselbrant I, Piitulainen E, Pettersson G, Magnusson P, Peterson B, Wollmer P, Leander P, Ekberg O, Akeson P. Hyperpolarized (3)he apparent diffusion coefficient mri of the lung: Reproducibility and volume dependency in healthy volunteers and patients with emphysema. *J Magn Reson Imaging* 2008;27:763-770.
85. Newell JD, Jr., Hogg JC, Snider GL. Report of a workshop: Quantitative computed tomography scanning in longitudinal studies of emphysema. *Eur Respir J* 2004;23:769-775.
86. Altes TA, Mata J, de Lange EE, Brookeman JR, Mugler JP, 3rd. Assessment of lung development using hyperpolarized helium-3 diffusion MR imaging. *J Magn Reson Imaging* 2006;24:1277-1283.
87. Waters B, Owers-Bradley J, Silverman M. Acinar structure in symptom-free adults by helium-3 magnetic resonance. *Am J Respir Crit Care Med* 2006;173:847-851.
88. Snider GL. Emphysema: The first two centuries--and beyond. A historical overview, with suggestions for future research: Part 2. *Am Rev Respir Dis* 1992;146:1615-1622.
89. Snider GL. Emphysema: The first two centuries--and beyond. A historical overview, with suggestions for future research: Part 1. *Am Rev Respir Dis* 1992;146:1334-1344.
90. Snider GL, Brody JS, Doctor L. Subclinical pulmonary emphysema. Incidence and anatomic patterns. *Am Rev Respir Dis* 1962;85:66-83.
91. Evans A, McCormack D, Ouriadov A, Etemad-Rezai R, Santyr G, Parraga G. Anatomical distribution of 3he apparent diffusion coefficients in severe chronic obstructive pulmonary disease. *J Magn Reson Imaging* 2007;26:1537-1547.
92. Fain SB, Panth SR, Evans MD, Wentland AL, Holmes JH, Korosec FR, O'Brien MJ, Fountaine H, Grist TM. Early emphysematous changes in asymptomatic smokers: Detection with 3he MR imaging. *Radiology* 2006;239:875-883.
93. Fichele S, Woodhouse N, Swift AJ, Said Z, Paley MN, Kasuboski L, Mills GH, van Beek EJ, Wild JM. MRI of helium-3 gas in healthy lungs: Posture related

variations of alveolar size. *J Magn Reson Imaging* 2004;20:331-335.

94. Madani A, Keyzer C, Gevenois PA. Computed tomography assessment of lung structure and function in pulmonary emphysema. *Eur Respir Mon* 2004;30:145-160.
95. Naunheim KS, Wood DE, Krasna MJ, DeCamp MM, Jr., Ginsburg ME, McKenna RJ, Jr., Criner GJ, Hoffman EA, Sternberg AL, Deschamps C. Predictors of operative mortality and cardiopulmonary morbidity in the national emphysema treatment trial. *J Thorac Cardiovasc Surg* 2006;131:43-53.
96. Beinert T, Brand P, Behr J, Vogelmeier C, Heyder J. Peripheral airspace dimensions in patients with copd. *Chest* 1995;108:998-1003.
97. Stolk J, Dirksen A, Van Der Lugt A, Hutsebaut J, Mathieu J, De Ree J, Reiberg JHC, Stoel BC. Repeatability of lung density measurements with low-dose computed tomography in subjects with alpha-1-antitrypsin deficiency-associated emphysema. *Invest Radiol* 2001;36:648-651.
98. Gevenois PA, Yernault JC. Can computed tomography quantify pulmonary emphysema? *Eur Respir J* 1995;5:843-848.
99. Suki B, Lutchen KR, Ingenito EP. On the progressive nature of emphysema: Roles of proteases, inflammation, and mechanical forces. *Am J Respir Crit Care Med* 2003;168:516-521.
100. Dirksen A, Dijkman JH, Madsen F, Stoel B, Hutchison DCS, Ulrik CS, Skovgaard LT, Kok-Jensen A, Rudolphus A, Seersholm N, et al. A randomized clinical trial of alpha-1-antitrypsin augmentation therapy. *Am J Respir Crit Care Med* 1999;160:1468-1472.